Economic and Social Modulations of Innate Decision-Making in Mice Exposed to Visual Threats

Zhe Li[1,2,3], Jiahui Wang[3], Yidan Sun[3], Jialin Li[3], Ling-yun Li[4], Ya-tang Li[2,3*]
[1]Academy for Advanced Interdisciplinary Studies, Peking University, Beijing, China
[2]Beijing Institute for Brain Research, Chinese Academy of Medical Sciences and Peking Union Medical College, Beijing, China
[3]Chinese Institute for Brain Research, Beijing, China
[4]Department of Neurobiology, School of Basic Medical Sciences, Capital Medical University, Beijing, China
*Correspondence: yatangli@cibr.ac.cn

Abstract

When confronted by predators, animals make innate decisions with rapid reaction times—a trait shaped by natural selection to maximize survival. However, rapid reactions are effective only when grounded in accurate judgments and appropriate choices, which often require cognitive control. To address how such choices are shaped, we developed a behavioral paradigm to investigate how threat intensity, reward value, and social hierarchy influence decision-making in foraging mice exposed to overhead visual threats. Using a machine learning-based approach, we classified defensive responses into four distinct decision types. We observed rapid habituation to repeated looming threats, with substantial inter-individual variability in the rate of habituation. Across both early and late phases of habituation, threat intensity is the primary determinant of decision-making, strongly driving behavior towards escape. In contrast, the influence of reward is context-dependent and emerges primarily in the late phase: under low-threat conditions, higher rewards suppress defensive responses, consistent with value-based decision theory, whereas under high-threat conditions, higher rewards promote escape, potentially reflecting heightened vigilance. Innate decision-making is further modulated by social hierarchy, with dominant mice showing greater vigilance and a stronger bias towards risk-averse behaviors, while subordinates are more reward-driven. To understand the underlying decision-making process, we developed a drift-diffusion leaky integrator model that successfully captures how threat intensity, reward value, and vigilance are integrated. Together, these findings reveal the economic and social modulation of innate decisions, offering insights into the computational mechanisms underlying the interplay between instinctive reactions and cognitive control.

Keywords: decision-making; innate responses; visual threat; reward value; social hierarchy; vigilance; drift-diffusion; leaky integrator

1 Introduction

How animals make decisions among alternative actions is a key question in neuroscience. In natural environments, decisions arise from the integration of sensory inputs, internal states, and learned experience (Meister, 2022). In the laboratory, both learned and innate paradigms have been used to study decision-making. Some learned paradigms, such as two-alternative forced choice (2-AFC) and GO-NOGO tasks (Andermann et al., 2010; Burgess et al., 2017), often require weeks of training

in head-fixed animals; whereas other learned paradigms require less training over several days in freely moving animals, including maze exploration (Barnes, 1979; Morris, 1984; Rosenberg et al., 2021; Small, 1901), foraging decisions (Hayden, 2018; Hayden et al., 2011; Steiner and Redish, 2014), and active avoidance (Bravo-Rivera et al., 2014; Moscarello and LeDoux, 2013; Mowrer and Lamoreaux, 1946). While these paradigms have significantly advanced our understanding of the neural mechanisms underlying learned decisions, the training itself may engage neural circuits that differ from those evolved for innate decision-making (Steinmetz et al., 2019).

In contrast, innate decisions—such as whether to escape from an approaching aerial predator (De Franceschi et al., 2016; Yilmaz and Meister, 2013) or a simulated ground threat like a robogator (Amir et al., 2015; Choi and Kim, 2010)—are executed without prior training and may more directly reflect the function of neural circuits shaped by natural selection. In complex environments, making correct and rapid innate defensive decisions often requires cognitive control to assess risk and evaluate alternative defensive strategies (Evans et al., 2019). Defensive responses to terrestrial predators have been well studied: escape decisions depend on predator–prey distance (Ydenberg and Dill, 1986), and the predatory imminence continuum theory describes a graded set of defensive behaviors tuned to perceived threat level (Fanselow and Lester, 1988). Responses to approaching aerial predators are likely also scaled with the perceived threat intensity, which depends on the physical properties of the threat (De Franceschi et al., 2016; Liden and Herberholz, 2008; Tammero and Dickinson, 2002; Yang et al., 2020; Yilmaz and Meister, 2013), prior experience (Vale et al., 2017), and environmental context, including housing conditions (Lenzi et al., 2022). At the neural level, the superior colliculus (SC) is a central node for processing looming-evoked defensive responses, with distinct output pathways mediating escape versus freezing (Evans et al., 2018; Shang et al., 2018; Wei et al., 2015; Zhou et al., 2019).

Despite this progress, important gaps remain. Mice are social animals, and most predator encounters occur during foraging, yet it is unclear how they weigh perceived risks and rewards when making defensive decisions, or how these decisions are influenced by social hierarchy. To address these questions, we developed an ecologically relevant behavioral paradigm to investigate decision-making in foraging mice exposed to overhead visual threats. Our findings demonstrate that defensive choices are jointly influenced by threat intensity, reward magnitude, and social hierarchy, providing a behavioral framework for future investigations into the neural mechanisms underlying cognitive control of innate decision-making.

2 Results

2.1 A behavioral paradigm for studying innate decision-making in mice

To investigate how animals make innate decisions in natural environments, we designed a behavioral paradigm to simulate the defensive behavior of foraging mice in the wild. In this paradigm, a group of 2–5 co-housed mice was placed in a nest, with each individual identified using a radio frequency identification (RFID) tag. Only one mouse was allowed to enter a linear arena to receive the reward delivered at the end. As the mouse approached the reward, an overhead expanding dark disc that mimics the approach of an aerial predator was triggered (Figure 1A), forcing the animal to decide whether to risk getting the reward or defend itself for safety. Behavioral data were recorded using a ground-mounted camera, and DeepLabCut was used to track the movements of the mouse's nose and tail base (Mathis et al., 2018) (Figure S1A). Compared to the exploratory phase, the presence of looming stimuli significantly increased the frequency of arena entries but decreased the duration of each visit (Figures 1B and 1C).

To identify distinct behavioral patterns in response to the looming stimuli, we defined 19 behavioral features from key body points of the mouse and fed them into a random forest classifier to predict its decisions (Figures 1D and S1B, see Methods and Materials). Animal decisions across 3861 trials were categorized into four types: direct escape (11.8%), escape after assessment (43.2%), freezing (5.8%), and no response (39.2%, Figures 1E and 1F). The classification model achieved an accuracy of 95% (Figure S1C). A key distinction between "assessment+escape" and "freezing" decisions was the duration of stationary behavior: mice that decided to freeze remained stationary significantly longer than those in the "assessment+escape" group (Figure 1G). Furthermore, the latency to flee differed significantly between "escape" and "assessment+escape" decisions (Figure 1H).

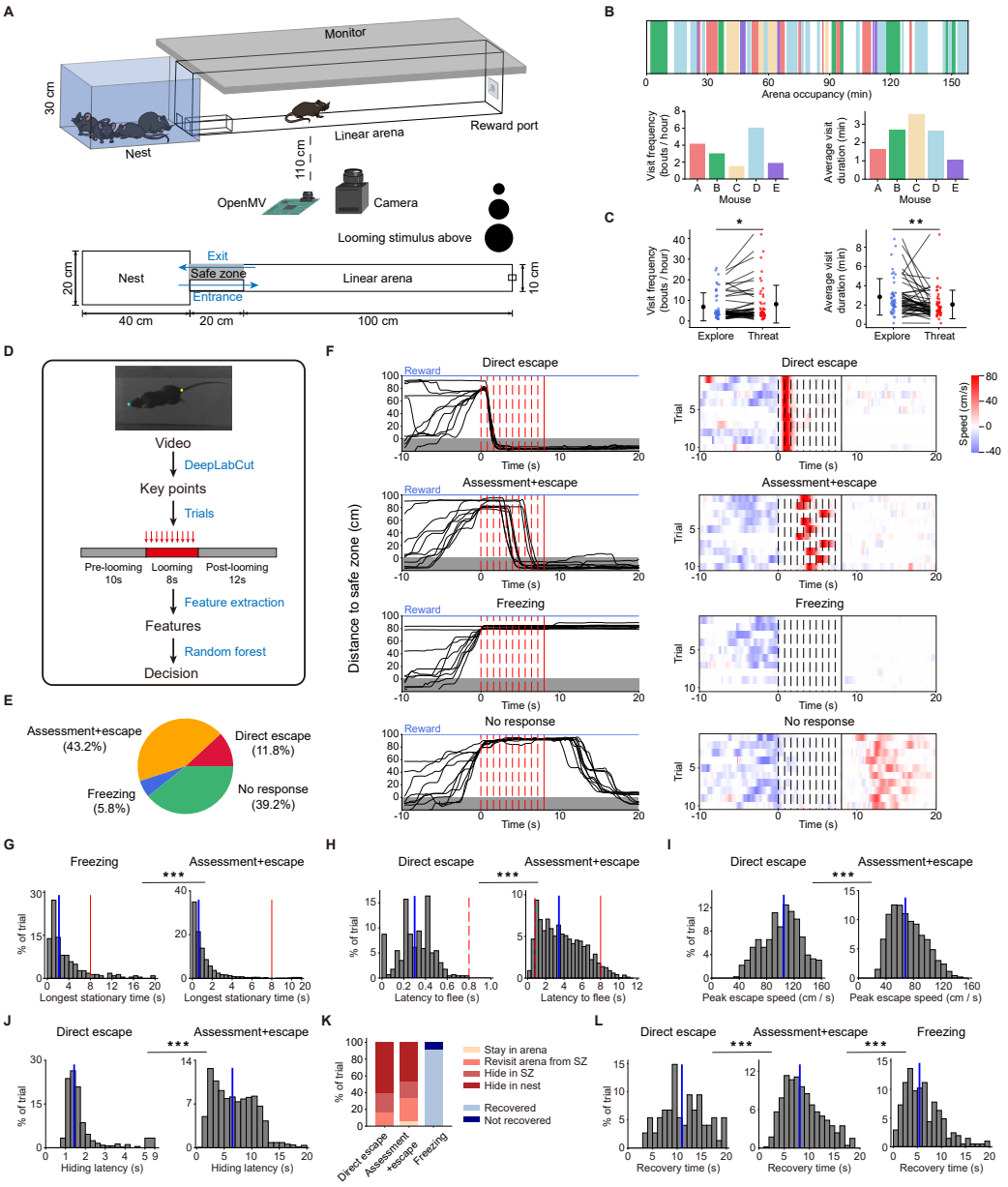

Figure 1: **A behavioral paradigm for investigating innate decision-making in mice.** (A) Schematic of the behavioral assay (3D and top-down views). (B) Top: arena occupancy patterns for five example mice in one session. Bottom: visit frequency and average duration for each visit. Colors mark the mouse's identity. (C) Visit frequency and duration under exploration and threat conditions. Error bars represent the standard deviation. N = 46 mice, paired *t*-test. (D) The pipeline for behavioral classification. (E) Distribution of decisions across 3862 trials from 140 mice. (F) Left: distance to the safe zone over time for four decision types (10 example trials each). Red dashed lines mark the onset of each stimulus repetition; solid lines mark the end of the last repetition. Grey shade indicates the safe zone. Right: locomotion speed towards the safe zone over time for the same trials. Positive speed indicates movement towards the safe zone. (G) Distribution of the longest stationary time for "freezing" and "assessment+escape". N = 224 and 1667 trials, Mann-Whitney-Wilcoxon test. Blue lines mark the median; red solid lines mark the end of the last repetition. (H) Distribution of latency to flee for "escape" and "assessment+escape". N = 458 and 1667 trials, Mann-Whitney-Wilcoxon test. Blue lines mark the median; red dashed and solid lines mark the end of the first and last repetitions, respectively. (I) Distribution of peak speed for "escape" and "assessment+escape". N = 458 and 1667, Mann-Whitney-Wilcoxon test. (J) Distribution of hiding latency in the safe zone for "escape" and "assessment+escape". N = 455 and 1563, Mann-Whitney-Wilcoxon test. (K) Distribution of post-decision behavioral states. (L) Distribution of fear recovery time for "escape", "assessment+escape", and "freezing". N = 74, 458, and 205, Kruskal-Wallis test followed by Dunn's post-hoc test with Holm correction. $^*p < 0.05$, $^{**}p < 0.01$, $^{***}p < 0.001$.

We hypothesized that fear level increases progressively across the decision types: "freezing", "escape after assessment", and "escape". This is supported by the observations that mice in the "escape" group exhibited higher flee speeds (Figure 1I) and shorter hiding latency (Figure 1J). Additionally, the proportion of mice that recovered within 20 seconds of the stimulus was about 20%, 40%, and 80% for "escape", "assessment+escape", and "freezing", respectively (Figure 1K). Consistently, recovery time decreased progressively across these decision types (Figure 1L). Our findings align with the theory of predatory imminence continuum (Fanselow and Lester, 1988), which proposes that defensive responses become more intense as the perceived threat level increases.

2.2 Mice make economic decisions modulated by vigilance

In the wild, most prey-predator encounters occur while prey animals are foraging, and prey have evolved to maintain high vigilance during foraging to enhance survival. Yet how food value, threat intensity, and vigilance interact to shape defensive decisions remains unclear. To address this question, we developed a behavioral assay that simulates how a foraging animal responds to an approaching aerial predator under different threat and reward conditions (Figure 2A). To maintain a consistent internal state across conditions, mice were not water-deprived. The higher reward value of sucrose over water was validated by measuring consumption during exploration (Figure S3A).

During the first trial, mice showed distinct trajectories and speed profiles across threat and reward conditions (Figures 2B and 2C). These patterns changed rapidly within the first 10 trials, indicating fast habituation to the looming stimulus. This learning was reflected in altered decision patterns (Figure 2D) and changes in escape distance, duration in the reward zone, peak escape speed, and latency to flee (Figures 2E–H). To account for both learning and individual variability, we segmented trials for each mouse into early and late phases using a change-point detection approach on the learning curves (Figures 2I, S3C, and S3D, see Methods and Materials).

In the early phase, behavior was shaped predominantly by the level of threat. Under higher threat, mice were more likely to choose direct escape behaviors (Figure 3A), with longer escape distances (Figure 3B) and less time spent in the reward zone (Figure 3C), suggesting a trade-off between threat avoidance and reward pursuit. Notably, latency to flee decreased with higher threat (Figure 3D), indicating heightened vigilance (Buck, 1966). This threat-dependent change in vigilance was further supported by the longer interval before re-entering the reward zone and slower foraging speed (Figures 3E, 3F, and S4), aligning with findings in birds that elevated predation risk increases vigilance and reduces feeding time (Caraco et al., 1980). In addition, escape speed increased significantly with threat (Figure 3G), reflecting the combined effects of perceived higher risk and heightened vigilance. The analyses restricted to the first trial yielded consistent results (Figures S5).

In the late phase, both threat level and reward value contributed to behavior. Threat remained a dominant factor, while reward exerted a significant, context-dependent influence. Under low-threat conditions, decisions were primarily driven by perceived reward value. As reward value increased, mice exhibited fewer defensive responses (Figure 3H), indicating that they weighed risk and reward to make economic decisions. Higher rewards led to shorter escape distance (Figure 3I) and longer stays in the reward zone (Figure 3J), supporting value-based decision-making strategies. In contrast, vigilance-related metrics, including latency to flee, foraging interval, and foraging speed, were largely unchanged across reward conditions (Figure 3K–M), suggesting that vigilance remains relatively stable. Consistently, escape speed decreased as reward value increased (Figure 3N). The value-based decision-making under low-threat conditions was further validated using within-subject comparisons to control for individual variability (Figure S6).

Under high-threat conditions, however, increasing reward value produced the opposite effect: mice showed more direct escape behaviors (Figure 3H). This shift in decision patterns can be attributed to heightened vigilance driven by reward, as evidenced by shorter latencies to flee, longer foraging intervals, and slower foraging speeds (Figures 3 K–M). This counterintuitive observation suggests that under high threat, reward value indirectly shapes decision-making by modulating vigilance. In contrast, duration in the reward zone did not increase with reward value (Figure 3J). Collectively, these findings reveal how innate decision-making in response to looming stimuli is shaped by the dynamic interplay between perceived threat intensity, reward value, and vigilance.

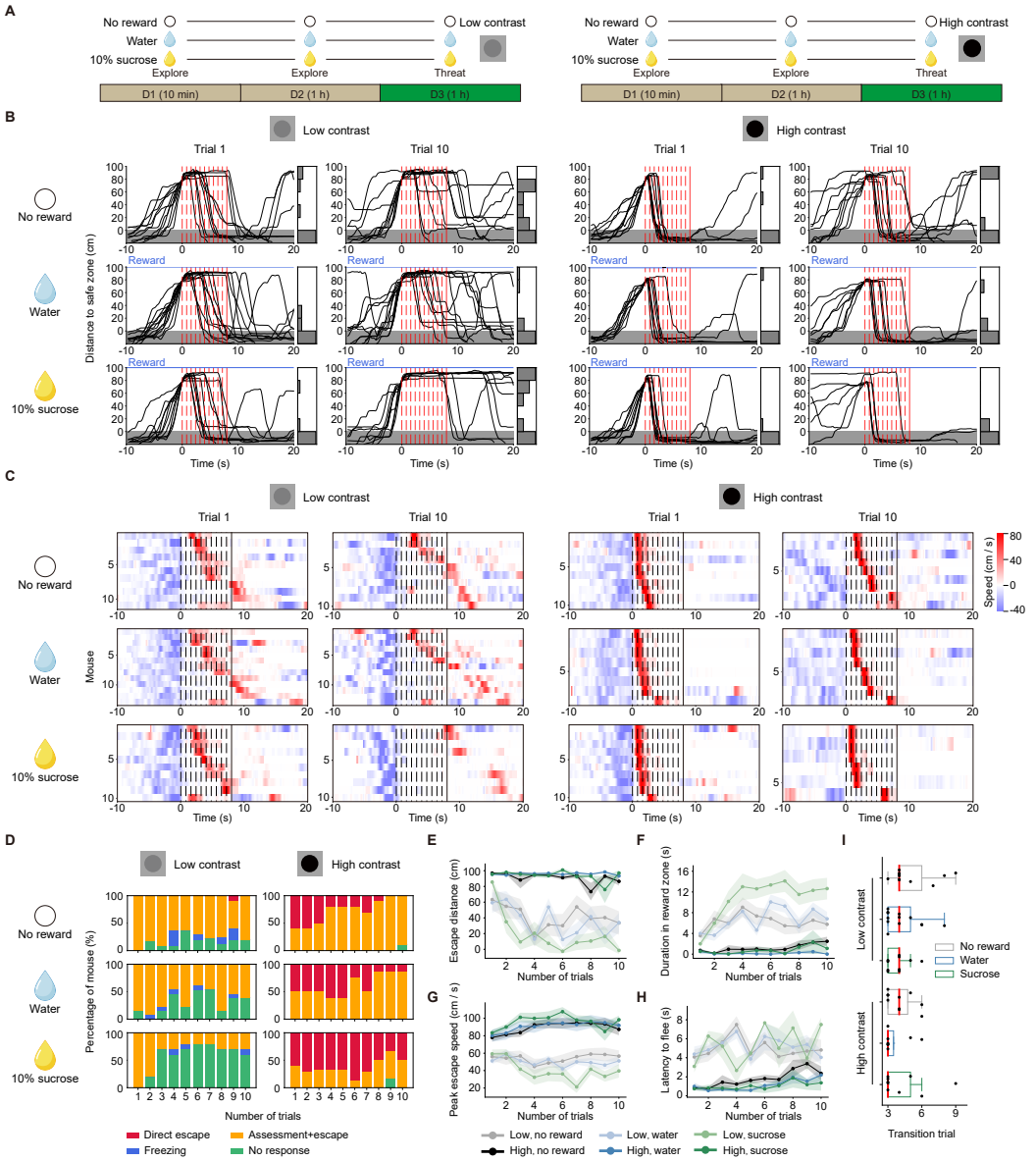

Figure 2: **Mice learn quickly from experience.** (A) Schematic of the behavioral assay for studying the economic modulation of innate decision-making. (B-C) Distance to the safe zone and locomotion speed over time for the 1st and 10th trials in response to low- and high-contrast looming stimuli across different reward conditions. Right inset in (B) is the distribution of distance to the safe zone at the end of each trial. Dashed lines mark the start of each stimulus, and solid lines mark the stimulus offset. N = 11 (no reward, low), 13 (water, low), 10 (sucrose, low), 10 (no reward, high), 8 (water, high), 10 (sucrose, high) mice. (D) Summary of the decisions across the first 10 trials under different risk and reward conditions. N = 11, 13, 10, 10, 8, 10 mice. (E-H) Escape distance under threat, duration in reward zone, peak escape speed, and latency to flee across trials in all conditions. Shade denotes the standard error of the mean. (I) Transition trials marking the shift between phases across conditions. Red lines indicate the median; boxes span the interquartile range (IQR); whiskers extend to 1.5 × IQR beyond the box.

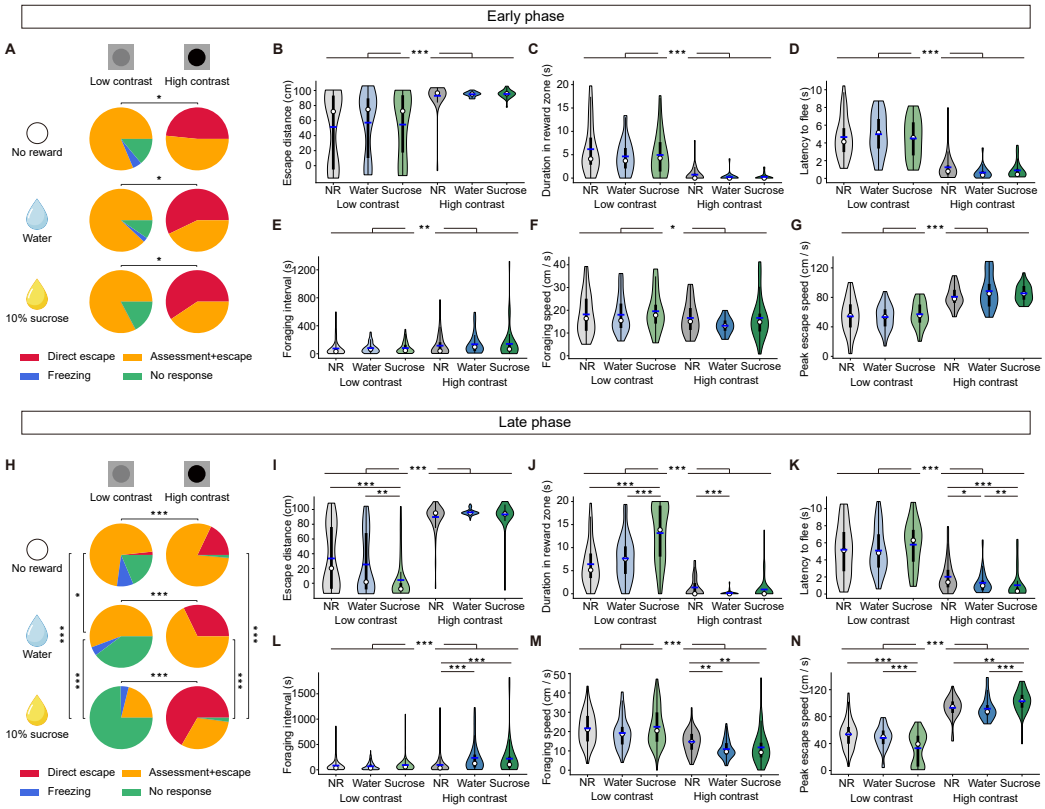

Figure 3: **Mice make economic decisions modulated by vigilance.** (A) Distribution of decisions in the early phase for six experimental conditions. N = 43 trials from 11 mice (none, low), 42 trials from 13 mice (water, low), 29 trials from 10 mice (sucrose, low), 31 trials from 10 mice (none, high), 21 trials from 8 mice (water, high) and 32 trials from 10 mice (sucrose, high), Chi-squared test. (B-G) Escape distance under threat, duration in the reward zone, latency to flee, foraging interval, foraging speed, and peak escape speed in the early phase across all conditions. Scheirer–Ray–Hare test with post hoc Dunn's test (Holm correction). N = 43, 42, 29, 31, 21, 32 trials for B, C, F, G; N = 35, 37, 24, 31, 21, 32 trials for D; N = 116, 84, 54, 58, 36, 48 intervals for E. (H) Distribution of decisions in the late phase for six experimental conditions. N = 59 trials from 11 mice (none, low), 88 trials from 13 mice (water, low), 71 trials from 10 mice (sucrose, low), 67 trials from 10 mice (none, high), 59 trials from 8 mice (water, high) and 48 trials from 9 mice (sucrose, high), Chi-squared test. (I-N) Escape distance under threat, duration in the reward zone, latency to flee, foraging interval, foraging speed, and peak escape speed in the early phase across all conditions. Scheirer–Ray–Hare test with post hoc Dunn's test (Holm correction). N = 59, 88, 71, 67, 59, 48 trials for I, J, M, N; N = 43, 49, 15, 66, 59, 47 trials for K; N = 116, 182, 114, 137, 71, 57 intervals for L. For all panels: $^{*}p < 0.05$, $^{**}p < 0.01$, $^{***}p < 0.001$.

2.3 Influence of social hierarchy on decision-making under threat

Mice are social animals that live in groups, where social hierarchy often plays a critical role in shaping behavior. To investigate how social rank influences decision-making under threat, we compared the responses of dominant and subordinate mice to looming stimuli. Rank within each mouse pair was determined using the tube test before and after the behavioral experiments (Figure 4A, see Methods and Materials), and only pairs with stable rankings were included in the analysis.

We first verified that behavioral responses to the visual threat were not confounded by the presence of a social partner. Before looming exposure, subordinate mice spent more time exploring the arena than dominant mice (Figures 4B and 4C), which may reflect social avoidance. However, this difference disappeared during and after looming exposure, suggesting that the looming stimulus became the primary driver of behavior. To confirm this, we examined the probability of mice fleeing to the nest. If subordinates were avoiding dominants, they should preferentially escape to the safe zone rather than return to the nest where the dominant was present. Contrary to this prediction, dominant and subordinate mice showed similar probabilities of fleeing directly to the nest (Figure 4D), confirming that defensive responses were driven by the visual threat rather than by social avoidance.

When the threat co-localized with the reward, only dominant mice reduced their relative time spent in the reward zone during the 2-h session (Figures 4E and 4F), indicating greater vigilance and risk aversion compared to subordinates. This heightened vigilance in dominant mice was further supported by reduced habituation to the looming threat (Figures 4G, 4H, and S7), a higher proportion of direct escape decisions (Figure 4I), and shorter latencies to flee (Figure 4J). No rank differences were observed in foraging interval or foraging speed. This may be due to the experimental design, in which only one mouse was allowed in the arena at a time, potentially altering natural foraging dynamics.

Furthermore, dominant mice prioritized threat avoidance over reward, fleeing longer distances with higher escape speed and spending less time in the reward zone (Figures 4M–O). To rule out the possibility that the tube test itself influenced defensive behavior, we conducted additional experiments in which looming sessions occurred both before and after the tube test (Figure S8); the results remained largely consistent. Together, these findings indicate that social hierarchy biases the trade-off between reward seeking and threat avoidance, with dominant mice exhibiting heightened threat vigilance and subordinate mice showing stronger reward-driven behavior.

2.4 A mathematical model for innate decision-making under threat

Our experimental results demonstrate that innate decision-making in response to visual threats is influenced by perceived threat intensity, reward value, and vigilance. To understand the underlying decision-making process, we developed a mathematical model in which the evidence for escape is accumulated by a drift-diffusion leaky integrator. An escape response is triggered when the evidence level crosses a predefined threshold:

$$\frac{dx_i}{dt} = -\alpha \cdot x_i(t) + \beta \cdot s(t) - r + \delta \cdot \frac{dW}{dt} \tag{1}$$

$$E(t) = \mathcal{H}\left(x_i(t) - x_{thr}\right) \tag{2}$$

Here, $x_i(t)$ is the accumulated escape evidence at time t on the ith trial. The leakage rate α drives the evidence towards zero and is the reciprocal of the integration time constant. The stimulus function $s(t)$ denotes the normalized diameter of the looming stimulus (Figure S9A). Together with the threat gain β, which reflects stimulus contrast and the animal's vigilance level, these terms represent the perceived threat level and drive evidence accumulation towards escape. The term r represents the perceived reward value, which suppresses the accumulation of escape evidence. $W(t)$ is a Wiener process, such that $W(t + \Delta t) - W(t) \sim \mathcal{N}(0, \Delta t)$, and δ is the diffusion rate. The binary variable $E(t)$ indicates whether an escape decision is made, with $\mathcal{H}$ denoting the Heaviside step function and x_{thr} the decision threshold. If a decision is reached within the first expansion of the looming disc, it is classified as a direct escape; otherwise, it is classified as an escape after assessment.

Model parameters were estimated using behavioral data in the late phase of reward-threat experiments in two steps (see Methods and Materials). First, we fit the model to the data under no-reward

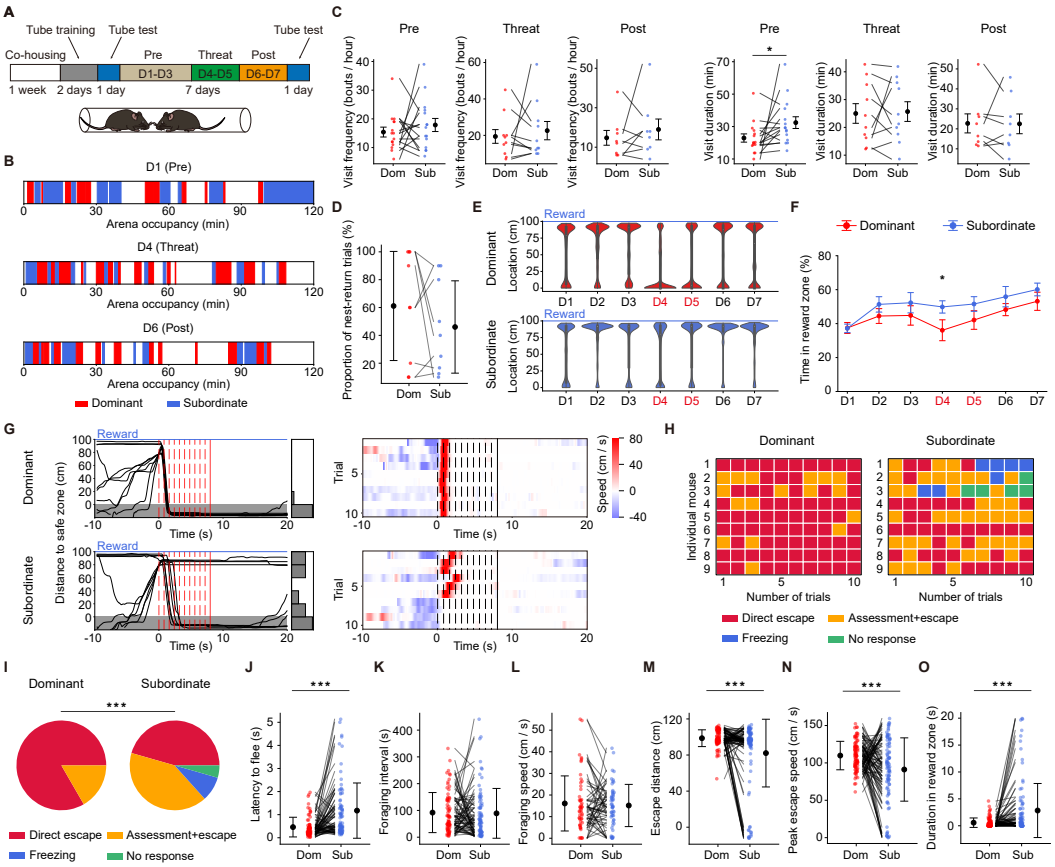

Figure 4: **Influence of social hierarchy on innate decision-making.** (A) Schematic of the behavioral assay for studying the social modulation of innate decision-making. Top, experimental timeline. Each session lasted 2 hours per mouse pair during the pre-looming, looming, and post-looming phases. Bottom, schematic of the tube test. (B) Arena occupancy for an example pair of mice during the three sessions. (C) Visit frequency and total visit duration for dominant and subordinate mice during the pre-threat, threat, and post-threat sessions. N = 5 pairs (pre), 5 pairs (threat), 4 pairs (post), respectively; paired *t*-test. (D) Proportion of nest-return trials in escape trials for dominant and subordinate mice. N = 9 pairs, paired *t*-test. (E) Distance to the safe zone over seven days for an example pair. Looming stimuli were presented on days 4 and 5. (F) Percentage of time spent in the reward zone across days. Error bars represent SEM. N = 9 pairs, paired *t*-test. (G) Distance to the safe zone (left) and locomotion speed (right) for an example pair. (H) Behavioral decisions across the first 10 trials for 9 mouse pairs. (I) Pie charts showing decision distributions for dominant and subordinate mice. N = 90, 90 trials, Stuart-Maxwell test. (J) Latency to flee for dominant and subordinate mice. N = 78 trials; paired *t* test. (K) Foraging interval for dominant and subordinate mice. N = 75 trials. (L) Foraging speed for dominant and subordinate mice. N = 53 trials. (M–O) Escape distance under threat, peak escape speed, and duration in the reward zone for dominant and subordinate mice. N = 90 trials. $^{*}p < 0.05$, $^{**}p < 0.01$, $^{***}p < 0.001$.

conditions and identified the optimal leakage rate ($\alpha = 1.78$), threat gain (low threat: $\beta = 1$; high threat: $\beta = 1.44$), diffusion rate ($\delta = 5.6$), and decision threshold ($x_{thr} = 0.71$) (Figure S9B). This revealed distinct decision-making dynamics under low- and high-threat conditions. Under low threat, the average evidence level remained below the escape threshold, and escape decisions emerged from stochastic fluctuations in individual trials (Figure 5A). Under high threat, the average evidence level crossed the threshold, indicating that escape decisions were mainly driven by threat gain (Figure 5B). Notably, threat gain and diffusion rate had distinct effects on latency to flee: threat gain shifted the mean latency, while diffusion rate affected its variance. Thus, the model captured not only the observed decision patterns but also the distributions of latency to flee.

In the second step, we identified the threat gain and reward value across different threat and reward conditions in the late phase (Figures S9C and S9D). Consistent with experimental findings that decisions under low threat were primarily driven by reward value, the fitted reward-value parameter increases with reward magnitude (0, 0.08, and 0.25 for no reward, water, and sucrose, respectively). With these parameters, the model reproduced the observed reduction in escape likelihood without changes in latency to flee (Figures 5A, 5C, and 5E). The same reward-value parameters were then used to model the decision-making process under high-threat conditions. The fitted threat-gain parameter increased across reward conditions (1.44, 1.8, and 2.55 for no reward, water, and sucrose, respectively), counteracting—and ultimately reversing—the influence of reward value. The model again reproduced the experimentally observed increase in escape decisions and decrease in latency to flee (Figures 5B, 5D, and 5F).

To assess the model's predictive power, we simulated how the decision score and latency to flee vary as functions of reward value (r) and threat gain (β). Increasing reward generally reduces escape probability and increases latency to flee, whereas increasing threat gain has the opposite effect (Figures 5G, 5H, and S9E–G). These relationships were confirmed by a simplified deterministic model (Figures S9H–K, see Methods and Materials). Notably, reward can also indirectly promote escape by elevating vigilance, with the magnitude of this effect depending on the level of baseline vigilance, defined as vigilance in the absence of reward (Figure 5I). This dual influence explains the absence of a reward effect in the early phase under both threat conditions: high vigilance shifts the operating range to a region where reward's indirect promoting effect is balanced by its direct suppressing effect on escape decisions.

We next applied this model to the social-threat paradigm. The behavior of dominant mice was captured by a combination of lower reward value and higher threat gain compared to subordinates (Figures 5G and 5H). This aligns with the experimental finding that dominant animals spent less time in the reward zone and fled more quickly (Figures 4J and 4O). Together, these results demonstrate that the model robustly captures key behavioral features across phases and paradigms, providing a unified mechanistic account of innate decision-making under threat (Figure 5J).

3 Discussion

When confronted by a predator, an animal must rapidly decide whether to escape, freeze, or continue its ongoing behavior. This life-or-death decision is crucial for rodents facing aerial predators. While mice are social animals and most predator encounters occur during foraging, it remains unclear how they integrate perceived risk and reward when making defensive decisions, or how these decisions are influenced by social hierarchy. Using a foraging-based paradigm, we demonstrate that responses to visual threat are shaped by threat intensity, reward value, social rank, and internal state, and this integrated decision process can be captured by a mathematical model.

3.1 Main findings

We designed a behavioral paradigm to simulate how mice respond to visual threats during foraging (Figure 1). Mice rapidly adapted to repeated looming threats, with substantial inter-individual variability in the rate of habituation (Figure 2). While threat intensity robustly shaped behavior in both early and late phases of habituation, reward exerted a clear influence only in the late phase (Figure 3). Specifically, increasing threat intensity shifted behavior towards more defensive responses. In contrast, reward value produced a context-dependent effect: under low-threat conditions, higher rewards suppressed defensive responses, aligning with value-based decision theory; whereas under high-threat conditions, higher rewards promoted escape decisions, potentially reflecting heightened

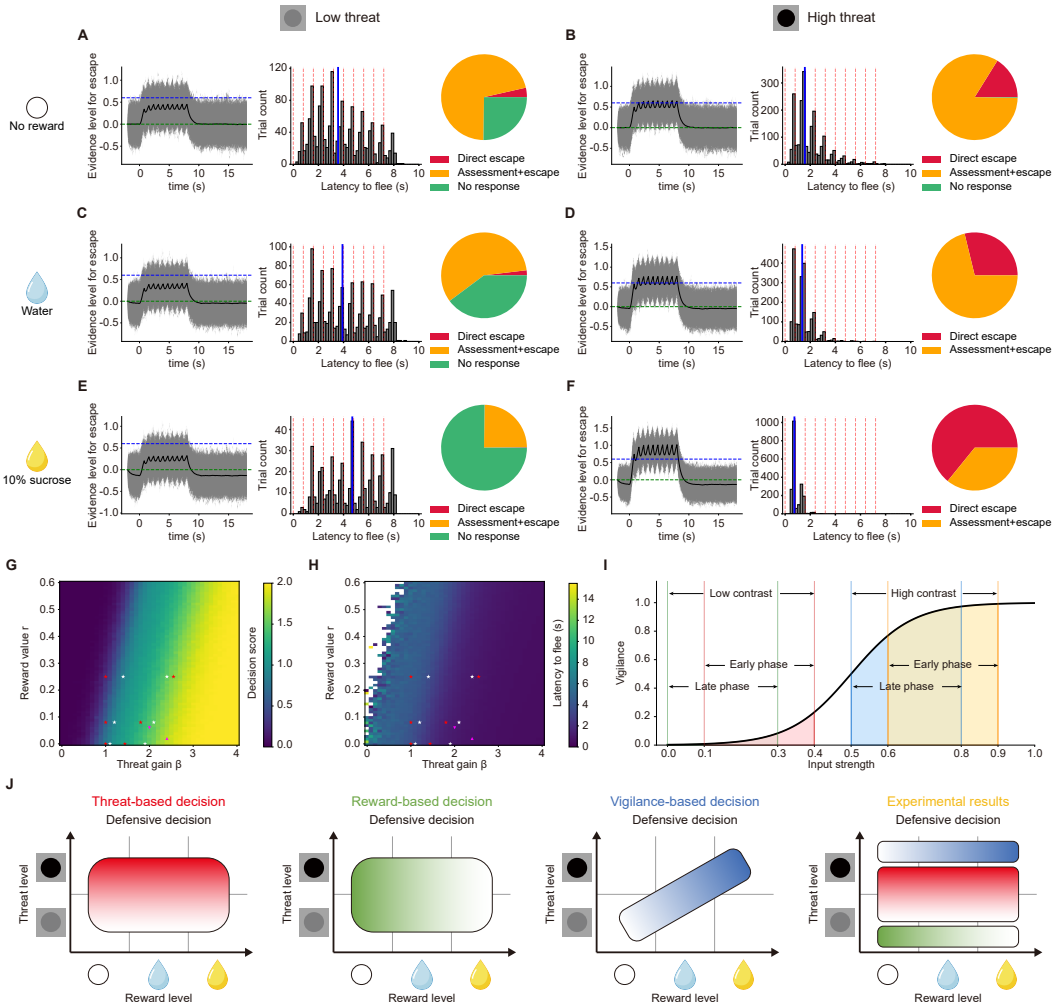

Figure 5: **Drift-diffusion leaky integrator model for escape decisions.** (A-F) Simulated accumulation of escape evidence, along with predicted latencies to flee and decision distributions across six threat and reward conditions. Green dashed horizontal lines mark the $x = 0$; blue dashed horizontal lines mark the $x = x_{thr}$; red dashed vertical lines mark the onset of each looming stimulus; blue vertical lines mark the median. (G) Heatmap of decision scores as a function of threat gain and reward value. White and red stars indicate fitted parameters for the early and late phases of the reward–threat paradigm, respectively; upward and downward pink triangles indicate fitted parameters for dominant and subordinate mice in the social-threat paradigm, respectively. (H) Heatmap of latencies to flee as a function of threat gain and reward value. (I) Vigilance as a function of input strength, illustrating how the indirect effect of reward on defensive decisions via vigilance depends on the baseline vigilance level. (J) Schematic showing how threat intensity, reward value, and vigilance jointly determine defensive decisions. Color saturation indicates the likelihood of defensive decisions.

vigilance. Innate decision-making was further shaped by social hierarchy (Figure 4): dominant mice exhibited a stronger tendency towards defensive behaviors, whereas subordinates were reward-driven and less likely to flee. Finally, we developed a drift-diffusion leaky integrator model to simulate the decision-making process, effectively capturing the key features of the observed decision patterns (Figure 5).

3.2 Relation to earlier work

Aerial predators pose a significant threat to rodents. Previous studies have shown that overhead visual stimuli in the laboratory elicit robust defensive behaviors in rodents (Wallace et al., 2013; Yilmaz and Meister, 2013). Because these stimuli can mimic distinct predatory actions, the resulting behavioral responses depend on the specific physical properties of the stimulus. For example, an overhead expanding dark disc that mimics an approaching aerial predator preferentially triggers escape rather than freezing (Yilmaz and Meister, 2013), while a small black moving dot that mimics a cruising predator predominantly induces freezing behavior (De Franceschi et al., 2016). These findings suggest that the response is not a simple reflex but involves a decision-making process. Additional stimulus properties that influence the action selection include contrast, speed, size, and shape (De Franceschi et al., 2016; Evans et al., 2018; Yang et al., 2020). Support for a decision-making process also comes from its modulation by environmental factors and experience: mice freeze more when no refuge is available (Wei et al., 2015) and quickly learn that the looming stimulus poses no real threat (Lenzi et al., 2022; Vale et al., 2017; Zhong et al., 2023). This innate decision-making process is observed across invertebrates and vertebrates (Evans et al., 2019).

Compared with earlier work, the present study differs in two aspects. First, instead of manually annotating behavioral responses, we employed a machine-learning approach to classify behavioral decisions. This approach largely reduced the labor required for labeling and minimized misclassifications due to inter-individual variability. Second, unlike previous studies using 2D arenas, we designed a 1D linear arena to simulate foraging conditions, where the nest and reward zone were separated by a long corridor. Decision patterns observed here were similar to those reported in 2D environments (Yang et al., 2020). Consistent with previous findings (Lenzi et al., 2022), mice quickly adapted to the looming stimulus after a few trials.

One concern with the linear arena design is that the looming stimulus is usually presented at the end of the arena, raising the possibility that mice simply retreat upon reaching a physical boundary. To address this, we presented the stimulus between the foraging mice and the nest (Figure S2A). Under this condition, mice quickly escape towards the nest—and thus towards the threat—rather than away from it (Figure S2B). This behavior indicates that their escape responses are not simple reflexes, but instead incorporate the safety of the nest into their decisions.

Fanselow and Lester's predatory imminence continuum theory posits that defensive behaviors are graded according to perceived threat level (Fanselow and Lester, 1988). To test whether this framework applies to aerial threats, we varied both prey–threat distance and prey–safety distance. As prey-threat distance increased, mice showed less direct escape behavior, with longer latencies to flee and slower escape speeds (Figures S2C–G), indicating that defensive responses scale with threat proximity. These effects cannot be explained by the failure to detect the stimulus at longer distances; if that were the case, foraging speed would remain unaffected. Instead, mice slowed as they approached the threat in the 75-cm condition (Figure S2D), reflecting lower fear compared to shorter distances. In contrast, prey-safety distance did not significantly influence defensive behaviors (Figures S2H and S2I). One interpretation is that once an aerial threat is detected, the urgency to escape overrides evaluation of refuge proximity. To further verify this, we introduced barriers that lengthened the return path to the nest. Even under these conditions, defensive behaviors remained unaffected by prey-safety distance (Figures S2J and S2K).

3.3 Economic and social modulations of innate decision-making under threat

Value-based decision-making—where choices arise from comparisons of the subjective value of expected outcomes—is a well-established framework for understanding behavior across species (Rangel et al., 2008). Prospect theory, which accounts for decision-making under risk in humans (Kahneman and Tversky, 1979), has been applied to learned decision-making in rodents (Constantinople et al., 2019). Here, we demonstrate that value-based decision-making also extends to innate defensive

behaviors: when confronted with threat, mice integrate perceived reward and threat value to make their decisions.

Importantly, perceived value is determined not only by stimulus physical properties but also by internal brain state. In the resting state, for example, perceived stimulus strength scales with physical intensity according to Weber–Fechner laws. In our paradigm, the perceived threat value is strongly modulated by vigilance, a state of heightened and sustained attention to potential danger. This vigilance-dependent modulation substantially alters how the same looming stimulus is evaluated and the resulting decisions.

Consistent with value-based evaluation, increasing threat intensity reliably increased defensive responses across reward conditions and behavioral phases. These changes reflect differences in perceived threat rather than stimulus detection, as evidenced by coordinated changes in escape latency, distance, and speed, and further supported by trial-by-trial inspection confirming reliable stimulus detection across contrast levels (Figure S5).

Reward-dependent behavior also follows value-based principles, but in a vigilance-dependent manner. In nature, foraging often occurs under predation risk, and evolutionary pressure has favored prey that maintain heightened vigilance in the presence of high-value rewards. Consistent with this, increasing the reward magnitude increased both perceived reward value and—via elevated vigilance—perceived threat value. These opposing effects jointly govern the escape decision.

In the early phase, baseline vigilance is already high because looming is an innate threat. Under this high-vigilance condition, reward-driven increases in perceived reward and perceived threat counterbalance each other, resulting in no behavioral differences across reward conditions. With repeated exposure, habituation to looming reduces vigilance, shifting the operating region leftward along a sigmoidal vigilance–intensity function (Figure 5I). Such a sigmoidal form is biologically plausible because vigilance is bounded by a relaxed-state minimum and by cognitive capacity. This shift has opposite consequences under low versus high threat. Under low threat in the late phase, reduced vigilance compresses the dynamic range, weakening the indirect effect of reward on perceived threat and allowing perceived reward value to dominate decisions. Under high threat, the vigilance function remains within a steeper region of the sigmoid, where increases in reward effectively elevate vigilance and thus perceived threat. As a result, reward produces the opposite behavioral effect under high threat. Together, these dynamics explain why reward effects are absent early but emerge after habituation in a strongly threat-dependent manner.

Social rank–dependent differences in defensive behavior also fit within this framework. Even under identical conditions, dominant mice perceived higher threat value due to higher vigilance and lower reward value, consistent with their more risk-averse behavior. Similar status-dependent escape patterns have been reported across species, including voles (Kleiman et al., 2014) and crayfish (Krasne et al., 1997), suggesting an evolutionarily conserved strategy.

Because vigilance declines with habituation, factors that modulate the rate of habituation also influence defensive behavior. Although individuals vary, several patterns are consistent. Mice habituate more rapidly under high-threat or high-reward conditions (Figure 2I). Dominant mice habituate more slowly than subordinates, consistent with their elevated vigilance (Figures 5H and S7A). Housing conditions also alter habituation: group-housed animals adapt more slowly to looming than single-housed animals, and dominant–subordinate pairs habituate even more slowly than group-housed mice (Figures 2I and S7A). These patterns indicate that stable social relationships sustain high vigilance and slow habituation—an evolutionarily conserved strategy that may enhance survival.

One limitation of the present study is that our experiments were conducted exclusively in male mice to avoid the confounding effects of behavioral variability associated with the female estrous cycle. Extending this paradigm to females—with careful control for estrous cycles—will provide a more comprehensive understanding of how economic and social factors modulate defensive decision-making.

3.4 A proposed role for the superior colliculus in value integration

What neural circuits underlie the economic and social modulations of decision-making under threat? A growing body of research implicates the SC as a key node in looming-evoked defensive behaviors (Evans et al., 2018; Shang et al., 2015; Wei et al., 2015). In parallel, reward is encoded by

dopaminergic neurons in the ventral tegmental area (VTA) (Cohen et al., 2012; Schultz, 1998) and serotonergic neurons in the dorsal raphe nucleus (Liu et al., 2014; Miyazaki et al., 2011), which project widely to regions such as ventral striatum (Schultz et al., 1992), orbitofrontal cortex (Tremblay and Schultz, 2000), cerebellum (Wagner et al., 2017). Furthermore, social status modulates behavior via circuits involving the medial prefrontal cortex (mPFC) (Kingsbury et al., 2019; Wang et al., 2011) and serotonergic signaling (Edwards and Kravitz, 1997; Raleigh et al., 1991; Yeh et al., 1997).

We propose the SC as a central hub for mediating the economic and social modulations of decision-making for several reasons. First, while neurons in the superficial (sSC) and intermediate (iSC) layers of the medial SC are involved in detecting looming threats and triggering defensive responses (Li et al., 2023, 2020), they also express receptors for both dopamine and serotonin (Mooney et al., 1996; Woolrych et al., 2021), indicating they can receive reward- and social-related information. Notably, dopamine receptor expression is layer-specific, with D1 receptors enriched in the sSC and D2 receptors in the iSC, suggesting layer-dependent processing of reward signals. Consistently, reward-related signals have been observed in the medial sSC (Baruchin et al., 2023). Second, the deep layers of SC receive from the retrosplenial cortex (RSC) (Campagner et al., 2023) and indirectly from the hippocampus (Benavidez et al., 2021), which may convey spatial and contextual information relevant to reward (Calvin et al., 2025). In parallel, the lateral SC mediates approach behaviors towards rewarding stimuli such as food or prey (Comoli et al., 2012; Krauzlis et al., 2013). These findings suggest that medial–lateral interactions within the SC may play a critical role in resolving threat–reward trade-offs during decision-making. Third, the deep-layer SC receives inputs from the mPFC (Benavidez et al., 2021), providing a pathway through which social and contextual signals can modulate defensive decisions. Finally, these SC deep layers are strongly and reciprocally connected with the periaqueductal gray (PAG) and project to dopaminergic neurons in the substantia nigra (Comoli et al., 2003), enabling efficient translation of integrated sensory, economic, and social signals into action execution. They also project to the lateral amygdala via the lateral posterior nucleus (LP) (Wei et al., 2015) to rapidly elicit the fear state.

Taken together, these anatomical and functional studies support the view that the SC serves as a central hub for the economic and social modulation of decision-making evoked by visual threat. In particular, cross-layer processing and medial–lateral interactions within the SC may provide key circuit mechanisms through which reward value and social context shape innate defensive decisions.

3.5 Mathematical modeling

The proposed drift-diffusion leaky integrator model builds on an integrator model of internal state (Gibson et al., 2015) and extends it by incorporating a reward-driven drift-diffusion process (Ratcliff, 1978). Conceptually, the integrator part in our model aligns with Lorenz's "hydraulic" model of motivation, which describes how internal drives shape behavior (Lorenz, 1950). While our model resembles the leaky integrator used to model escape behavior in flies (Gibson et al., 2015), it differs in several ways. First, the earlier model lacks a reward-related drift component. Second, while they modeled the looming effect as a delta function, our model allows the evidence level to vary continuously with the stimulus size. Third, the influence of vigilance is absent in that model. A similar model has been proposed (Evans et al., 2018), but it did not incorporate reward and vigilance. Note that the evidence level for escape in our model is not equivalent to the fear level (Anderson and Adolphs, 2014); rather, when it crosses a threshold, the animal may enter a fear state.

Below, we briefly discuss the roles of individual parameters. The leakage rate α represents a drive towards the resting state. Perceived threat was modeled as the product of the threat gain β and the sensory input $s(t)$ and promotes escape decisions, whereas perceived reward r drives the decision away from escape. The threat gain increases not only with threat intensity but also with reward value via its influence on vigilance. The effect of reward on vigilance depends on the operating region of the sigmoidal vigilance function. This operating region is set by the baseline vigilance level (Figure 5I) and reflects habituation to repeated looming threats. Furthermore, threat gain and reward value have distinct effects on escape latency: higher threat gain exponentially shortened latency, whereas higher reward value increased it linearly (Figure S9F and S9G). These effects are confirmed using a simplified deterministic version of the model (Figure S9J and S9K; see Methods and Materials).

Lastly, the diffusion rate δ plays a critical role, particularly under low-threat conditions where the average evidence trajectory fails to reach the threshold. This parameter may reflect the fluctuation of the animal's internal state. The diffusion rate captures the trial-to-trial variability: even small

amounts of noise can accumulate over time, resulting in large differences across individual trials and contributing to variability in escape latency. Overall, this computational framework not only accounts for our experimental observations but also offers a quantitative foundation for studying innate decision-making across species. Understanding how these parameters are implemented at the circuit level is an exciting direction for future research.

4 Methods and Materials

4.1 Animal

Male C57BL/6J mice were group-housed on a 12-hour light / 12-hour dark cycle and used at ages 2-3 months. Behavioral experiments were conducted during the light phase. All experimental procedures were performed under the animal welfare guidelines and approved by the Institutional Animal Care and Use Committee at the Chinese Institute for Brain Research, Beijing.

4.2 Behavioral platform

The behavioral platform consisted of a nest, a linear arena, a radio frequency identification (RFID) system, a real-time mouse position detection system, and a reward delivery port. As illustrated in Figure 1A, the nest (40 cm (L) $\times$ 20 cm (W) $\times$ 30 cm (H)) and the linear arena (100 cm $\times$ 10 cm $\times$ 30 cm) were made with infrared transmitting acrylic to allow unobtrusive behavioral monitoring. They were connected by a one-way tunnel (20 cm $\times$ 3 cm $\times$ 3 cm) for entering the arena and a 20 cm $\times$ 5 cm $\times$ 30 cm safe zone with a 5 cm $\times$ 5 cm one-way door for returning to the nest. Because it wasn't directly under the monitor, the safe zone was darker than the arena. Mice were labeled via implanted RFID tags, which were detected by an RFID reader placed around the tunnel. Only one mouse was allowed to enter the arena at a time. Specifically, when all mice were in the nest, the door between the nest and the tunnel was open, while the door between the tunnel and the arena remained closed. When a single mouse entered the tunnel, as detected by the RFID system, the door to the nest closed and the door to the arena opened, allowing the mouse to enter the arena. The mice were rewarded at the end of the arena with water or sucrose. Licking time and reward volume were recorded.

To track mouse position in real time, an OpenMV camera with a 90° field-of-view lens was mounted on the ground, 110 cm beneath the arena. The mouse position was used to control the tunnel doors and to trigger stimulus presentation when the mouse entered the arena. Specifically, the tunnel had two doors: the first connected the tunnel to the nest, and the second door connected the tunnel to the arena. Once a mouse entered the tunnel, the first door closed and the second door opened. A second camera (LBAS-U350-74M) with a lens (FA0615A) was also placed on the ground to record animal behavior at 30 frames per second.

4.3 Visual stimulation

Looming stimuli were presented on a 55-inch monitor (121 cm $\times$ 68 cm) suspended 32 cm above the arena. Visual stimulation was implemented using Psychopy in Python and was aligned to the mouse's real-time location. The stimulus was a black disc that expanded ten times on a gray background ($\sim$ 65 cd / cm^2). For each time, the disc expanded from 0° to 20° of visual angle at a speed of 40°/s, followed by a stationary phase lasting 0.3 s. The inter-stimulus interval was randomized between 1 and 2 minutes. Two stimulus contrasts at 20% and 99% were displayed by adjusting the luminance of the disc.

4.4 Economic modulation of innate decision-making

All mice were habituated to the behavioral platform for two days before the looming experiment. On the first day, five mice from the same home cage were placed in the nest for 30 minutes with all doors closed. Each mouse was then placed individually in the nest and allowed to explore the arena for 10 min under normal door operation; if a mouse entered the arena fewer than two times, the exploration period was extended until at least two arena visits were completed. Subsequently, all five mice were returned to the nest with all doors open and allowed to freely explore the arena for 2 h to ensure that each mouse learned the reward location at the end of the linear arena. On the second day, each mouse was placed individually in the nest and given an additional 1 h of exploration under normal door operation to further acclimate to the environment. The looming experiment was conducted the following day. An overhead looming stimulus of either low (20%) or high (99%) contrast was triggered when the mouse entered the trigger zone, defined as the region within 20 cm of the reward port. For each mouse, both the looming contrast and reward type remained constant across trials. In total, we collected and analyzed behavioral data from 590 trials across 62 mice.

To control for individual variation in decision-making, we compared the same animal's behavior under reward and no-reward conditions. Two groups of mice were used in the experiment. In the first group (n = 5), mice were first tested under the reward condition, followed by the no-reward condition. In the second group (n = 4), the order was reversed. For the reward condition, mice were water-deprived one day before the exploration, and water was provided via the reward port. In the no-reward condition, mice were not water-deprived, and the reward port was removed. Before the looming experiment, mice were acclimated to the linear arena for two days as described above. On the third day, a looming stimulus with 20% contrast was displayed for five trials. In total, behavioral data from 84 trials across nine mice were recorded and analyzed.

4.5 Social modulation of innate decision-making

To investigate the impact of social hierarchy on decision-making, we first determined the social rank of each mouse pair using the tube test (Wang et al., 2011). Mice were co-housed with a glass tube (3 cm diameter, 10 cm long) for one week, then trained to cross a 30 cm tube 10 times per day over two consecutive days. On the third day, a pair was tested for up to six trials; if one mouse achieved four consecutive wins, it was designated the dominant individual; otherwise, the pair (1 out of 6 pairs) was excluded from further experiment.

Before the looming experiment, mice were water-deprived and allowed to explore the linear arena for two hours per day over three days, during which water rewards were delivered at the end of the arena. Over the following two days, the looming experiment with a stimulus contrast of 99% was performed for two hours per day. After the looming experiment, mice continued to explore the arena for an additional two days, after which their social rank was reassessed with the tube test. All remaining pairs maintained a stable rank order.

To assess whether the tube test itself influenced defensive decision-making, additional looming experiments were conducted on four mouse pairs before and after introducing the tube test. Specifically, the first looming experiment was conducted prior to the tube test in Figure 4A. The behavioral patterns in a total of 180 trials from 18 mice were recorded and analyzed.

4.6 Behavioral quantification

Animal behaviors were quantified in three steps. First, two key points—the nose and tail base—were labeled and tracked in the recorded videos using DeepLabCut (Figure S1A). Tracked points with likelihood scores below 0.6 were excluded and filled via linear interpolation. Locomotion speed was calculated for each frame and smoothed using a 0.3 s moving average window. Unless otherwise specified, the speed of the tail base was used for subsequent analyses. Second, individual 30 s trials were extracted, each consisting of 10 seconds before, 8 seconds during, and 12 seconds after the looming stimulus. Multiple episodes of these states could occur within a single trial.

Third, we defined 19 behavioral features related to locomotion speed, distance, and state transitions. Eleven features were related to speed and distance: (1) peak speed towards the reward port before stimulus onset; (2-4) maximum, mean, and coefficient of variation of speed after stimulus onset; (5) latency to peak speed; (6) hiding latency, defined as the time between stimulus onset and arrival at the safe zone (set to 20 s if the mouse did not reach the safe zone by the end of the trial); (7) escape distance, defined as the distance covered between stimulus onset and offset; (8) distance to the nest at the end of the trial; (9) total distance traveled at speeds greater than 90% of the peak speed; (10) duration of movement at speeds greater than 90% of the peak speed; and (11) duration of time with both key points moving slower than 1 cm / s. Eight features were related to state transitions: (12) latency to flee, defined as the time from stimulus onset to the first escape state, where an escape state was identified when the animal moved more than 10 cm at a speed exceeding 10 cm / s; (13-15) average speed, distance traveled, and acceleration during the fastest escape episode; (16) latency to the fastest escape episodes; (17) latency to the first stationary state, where a stationary state was defined when both key points moved less than 1 cm / s for more than 0.3 s; (18,19) total and longest stationary duration.

Finally, these features were fed into a random forest model with a maximum depth of 5 to classify animal behaviors. For trials in which neither escape nor stationary states were identified, latencies (feature 12,16,17) were set to 20 s, distance (14) to 0 cm, speed (13) to 0 cm / s, acceleration (15) to 0 cm / s^2, and duration (18,19) to 0 s. The model was trained on 238 trials and tested on 102 trials,

achieving an accuracy of 0.95 on the test set. Using this classifier, behavioral decisions in 3862 trials across 140 mice were categorized into four types: direct escape, escape after assessment, freezing, and no response (Figure S1). A decision score was calculated for each condition as $S = 3p_e + 2p_{fe} + p_f$, where p_e, p_{ae}, p_f denote the proportion of direct escape, escape after assessment, and freezing, respectively. To quantify how quickly animals recovered from a fear state, we measured recovery time. For escape trials, recovery time was defined as the hiding duration, measured from entry into the safe zone to re-entry into the arena. For freezing trials, recovery time was defined as the interval between the onset of the first freezing episode and the termination of the last freezing episode.

To quantify the influence of reward, the reward zone was defined as a region within 10 cm of the reward port, and the duration in the reward zone was defined as the time spent within this zone during the 20 seconds following stimulus onset. Vigilance was assessed using latency to flee, foraging interval (time between two consecutive entries into the trigger zone), and foraging speed (average speed heading to the trigger zone before the looming exposure).

To segment the trials into two phases, we performed principal component analysis on a feature matrix containing decision score, escape distance, time spent in the reward zone, peak escape speed, and latency to flee across the first 10 trials. We extracted the first principal component (Figure S3), which captured the majority of the variance, and used its learning curve to detect transitions in behavior. Change points of the learning curve were detected by the ruptures approach (Gallistel et al., 2004; Truong et al., 2020).

4.7 Behavioral modeling

Parameters in the drift-diffusion leaky integrator model were estimated in two steps by minimizing a loss function using a grid search. In the first step, we fit our model to behavioral data in the no-reward condition, setting $r = 0$ and $\beta = 1$ for the low-threat condition, and estimated α, δ, x_{thr}, and β for the high-threat condition. In the second step, we estimated β and r for water and sucrose conditions under both threat conditions. The loss function combines fitting errors in the distribution of behavioral decisions ($\mathcal{L}_{\text{dec}}$), the median latency to flee ($\mathcal{L}_{\text{med}}$), and the variability of latency ($\mathcal{L}_{\text{sd}}$):

$$\mathcal{L} = 100\mathcal{L}_{\text{dec}} + 2\mathcal{L}_{\text{med}} + \mathcal{L}_{\text{sd}} \tag{3}$$

The decision-distribution mismatch is quantified using a mean cosine distance:

$$\mathcal{L}_{\text{dec}} = \frac{1}{C}\sum_{c=1}^{C}(1 - \frac{\mathbf{d}_c \cdot \hat{\mathbf{d}}_c}{\|\mathbf{d}_c\|\|\hat{\mathbf{d}}_c\|}) \tag{4}$$

where $\mathbf{d}_c$ and $\hat{\mathbf{d}}_c$ denote the observed and model-predicted decision distributions for contrast level c, and $C = 2$ is the number of threat conditions.

The median-latency loss is defined as

$$\mathcal{L}_{\text{med}} = \frac{1}{C}\sum_{c=1}^{C}\frac{\left|\hat{L}_c^{\text{med}} - L_c^{\text{med}}\right|}{\hat{L}_c^{\text{med}} + L_c^{\text{med}}}, \tag{5}$$

and the latency-variability loss is

$$\mathcal{L}_{\text{sd}} = \frac{1}{C}\sum_{c=1}^{C}\frac{\left|\hat{L}_c^{\text{sd}} - L_c^{\text{sd}}\right|}{\hat{L}_c^{\text{sd}} + L_c^{\text{sd}}}. \tag{6}$$

For the final fitted model (Equation 1), $\alpha = 1.78$ and $\delta = 5.6$. Under low-threat conditions, $\beta = 1$ for all conditions; under high-threat conditions, $\beta = 1.44, 1.8, 2.55$ for no reward, water, and sucrose, respectively. The reward values were $r = 0, 0.08, 0.25$ for no reward, water, and sucrose, respectively, under both threat conditions. In Equation 2, the decision threshold was $x_{thr} = 0.71$.

To further understand how threat and reward shape decisions, we analyze a deterministic simplification of the model:

$$\frac{dx}{dt} = -\alpha \cdot x(t) + n \cdot t - p \tag{7}$$

where $p > 0$ denotes the perceived reward value and $n \cdot t < 0$ denotes the perceived threat strength, which grows linearly over time.

With the initial condition $x(0) = 0$, the solution is

$$x(t) = \frac{n}{\alpha}t + \left(\frac{p}{\alpha} + \frac{n}{\alpha^2}\right)\left(e^{-\alpha t} - 1\right) \tag{8}$$

This reveals a competition between two components. First, a linear term driven by threat accumulation promotes escape over time. Second, an exponentially decaying component reflects the combined influence of reward and threat.

4.8 Quantification and statistical analysis

No statistical method was used to predetermine sample size. The Shapiro-Wilk test was applied to assess the normality of data distributions. For comparison between two groups, a two-sample *t*-test or paired *t*-test was used for normally distributed data; otherwise, the Mann–Whitney U-test or one-sample Wilcoxon signed-rank test was applied. For multi-group comparisons, one-way or two-way analysis of variance (ANOVA) was used when data were normally distributed, followed by Tukey's post hoc test. For non-parametric multi-group comparisons, the Kruskal–Wallis test (for one factor) or the Scheirer–Ray–Hare test (for two factors) was applied, followed by Dunn's post hoc test with Holm correction. The chi-square test was conducted to analyze categorical variables, while paired categorical comparisons were assessed using the Stuart–Maxwell test. Detailed statistical information for each experiment is provided in the Results section and figure legends.

Acknowledgments

We thank Lei Zhang, Xueting Sun, Haojun Sang, Qun Zhang, Bing Zhao, and Zhuofan Li in the CIBR instrumentation core for their help in designing and building the linear arena. Ling-yun Li is supported by the Natural Science Foundation of Beijing Municipality (5244028), the National Natural Science Foundation of China (32471071), and the R&D Program of Beijing Municipal Education Commission (1240030201). Ya-tang Li is supported by the National Natural Science Foundation of China (32271060), the Natural Science Foundation of Beijing Municipality (IS23073), and the start-up fund from CIBR.

Author contributions

Ya-tang Li supervised the project; Ya-tang Li, Zhe Li, and Yidan Sun designed the experiments; Zhe Li collected all the data; Zhe Li, Jiahui Wang, and Jialin Li analyzed the data; Ya-tang Li carried out the neural modeling; Zhe Li and Ya-tang Li prepared figures; Ya-tang Li, Ling-yun Li, and Zhe Li wrote the manuscript.

Data and Code Availability

Data and code are available in a public GitHub repository (`https://github.com/YatangLiLab/Li_Innate_Decision_Making_2025`).

Declaration of interests

The authors declare no competing interests.

5 Supplemental information

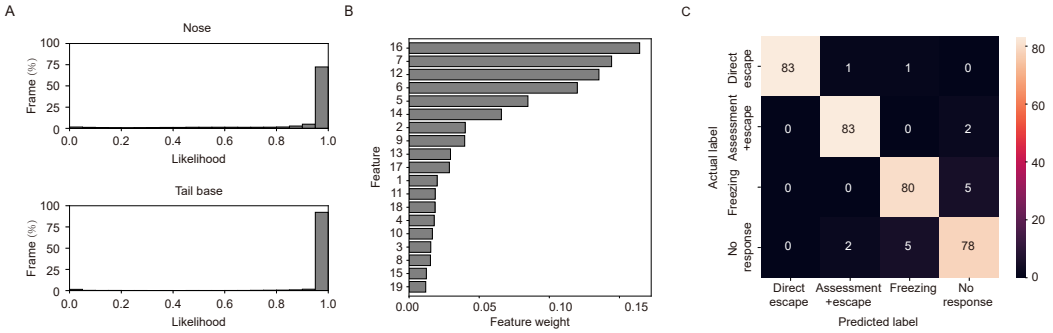

Figure S1: **Model validation and feature analysis for automated behavioral classification.** (A) Tracking accuracy of the mouse nose and tail base using DeepLabCut. (B) Weights of the 19 behavioral features in the random forest classifier. (C) Model performance evaluated by a confusion matrix on the test dataset.

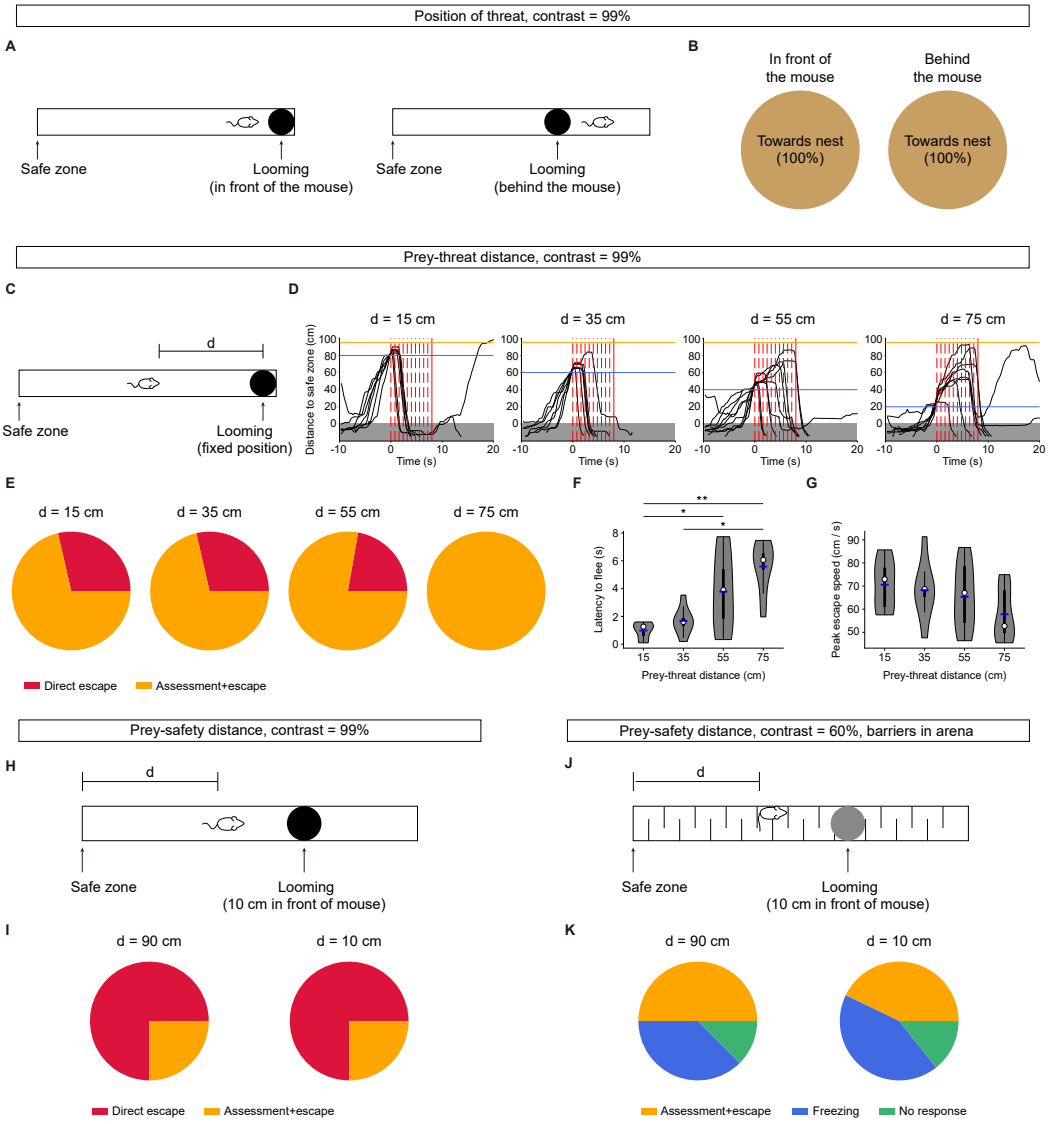

Figure S2: **Effects of threat position, prey–threat distance, and prey–safety distance on defensive responses to looming stimuli.** (A) Schematic of the experiment in which looming stimuli were presented either in front of or behind mice during foraging. (B) Distribution of escape direction for front and behind stimulus positions. N = 97, 16 trials. (C) Schematic of the experiment in which looming stimuli were presented at the end of the linear arena with varying distances between the mouse and the threat. (D) Distance to the safe zone over time for four prey-threat distances. Red dashed lines mark the onset of each stimulus repetition; solid lines mark the end of the last repetition. Grey shade indicates the safe zone. Blue lines mark the mouse's position when the looming stimulus was triggered; orange lines mark the location of the looming stimulus. N = 7 (15 cm), 7 (35 cm), 9 (55 cm), and 8 (75 cm) trials from 5 mice. (E) Distribution of decisions across prey-threat distances. (F–G) Latency to flee and peak escape speed across prey-threat distances. Kruskal-Wallis test with post hoc Dunn's test (Holm correction). (H) Schematic of the experiment in which looming stimuli were presented in front of the mouse at varying distances between the mouse and the safe zone. (I) Distribution of decisions across prey-safety distances. N = 4, 4 trials. (J) Schematic of the experiment in which low-contrast looming stimuli were presented at varying distances between the mouse and the safe zone in the linear arena with barriers. (K) Distribution of decisions across prey-safety distances in the barrier condition. N = 8, 7 trials. $^*p < 0.05$, $^{**}p < 0.01$.

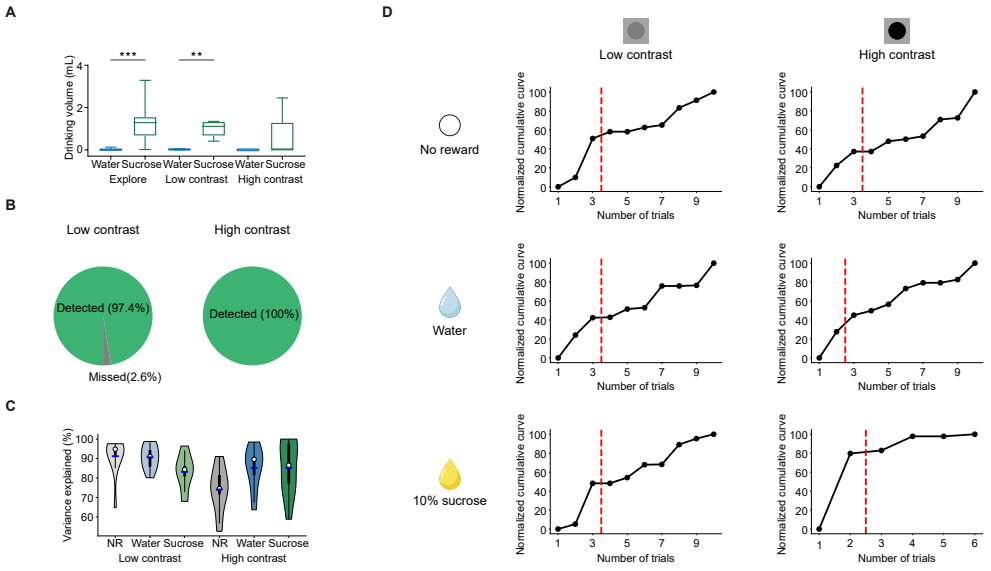

Figure S3: (A) Water or sucrose consumption during exploration and looming experiments at low and high contrasts. N = 10, 10, 5, 5, 5, 5 sessions; Mann–Whitney–Wilcoxon test. Boxes represent the interquartile range (IQR), and whiskers show the full data range. (B) Pie chart showing the proportion of looming stimuli detected by mice in no-response trials under low- and high-threat conditions. Low contrast: N = 117 trials from 29 mice; high contrast: N = 2 trials from 2 mice (high contrast). (C) Proportion of total behavioral variance explained by principal component 1 (PC1) for individual mice across all conditions. N = 11, 13, 10, 10, 8, 10. (D) Cumulative PC1 score for an example mouse in each condition. Red dashed lines mark the transition from the early to the late phase. $*p < 0.05$, $**p < 0.01$.

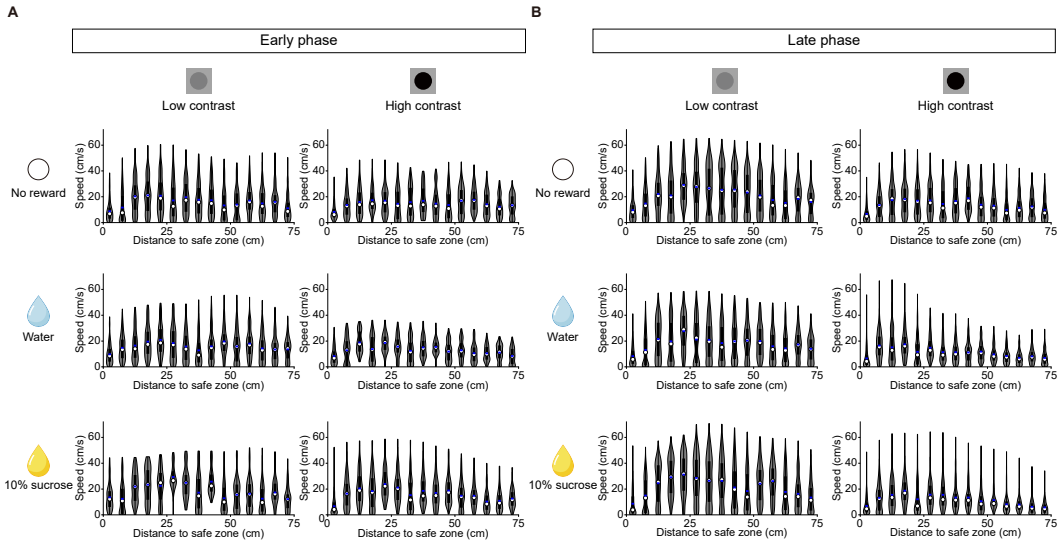

Figure S4: **Distribution of foraging speed.** (A) Distribution of foraging speed relative to distance from the safe zone in the early phase across different risk and reward conditions. (B) Distribution of foraging speed in the late phase. Data are from 11 mice (no reward, low contrast), 13 mice (water, low contrast), 10 mice (sucrose, low contrast), 10 mice (no reward, high contrast), 8 mice (water, high contrast), and 10 mice (sucrose, high contrast).

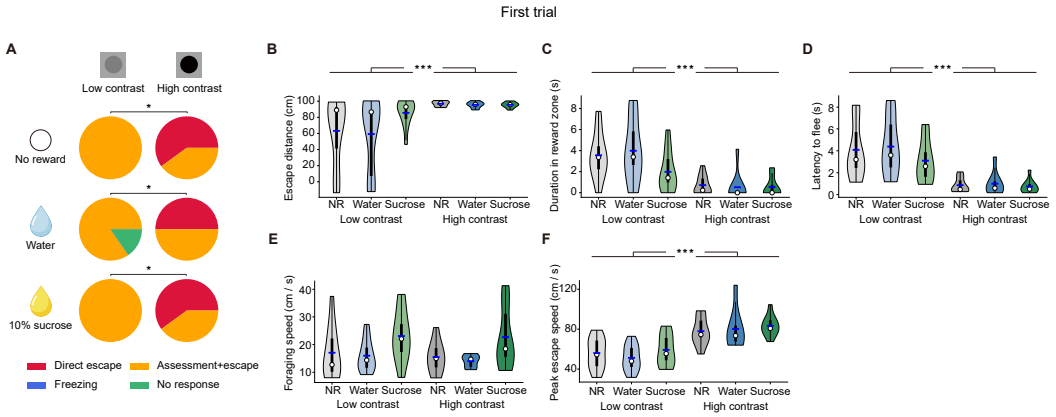

Figure S5: **Behavioral responses to looming stimuli across risk and reward conditions in the first trial.** (A) Distribution of decisions for each mouse under six conditions. N = 11 (no reward, low contrast), 13 (water, low contrast), 10 (sucrose, low contrast), 10 (no reward, high contrast), 8 (water, high contrast), 10 (sucrose, high contrast); Chi-squared test. (B–F) Escape distance under threat, duration in the reward zone, latency to flee, foraging speed, and peak escape speed across conditions. Scheirer–Ray–Hare test with post hoc Dunn's test (Holm correction). N = 11, 13, 10, 10, 8, 10 trials for B, C, E, F; N = 11, 11, 10, 10, 8, 10 trials for D. $^{*}p < 0.05$, $^{***}p < 0.001$.

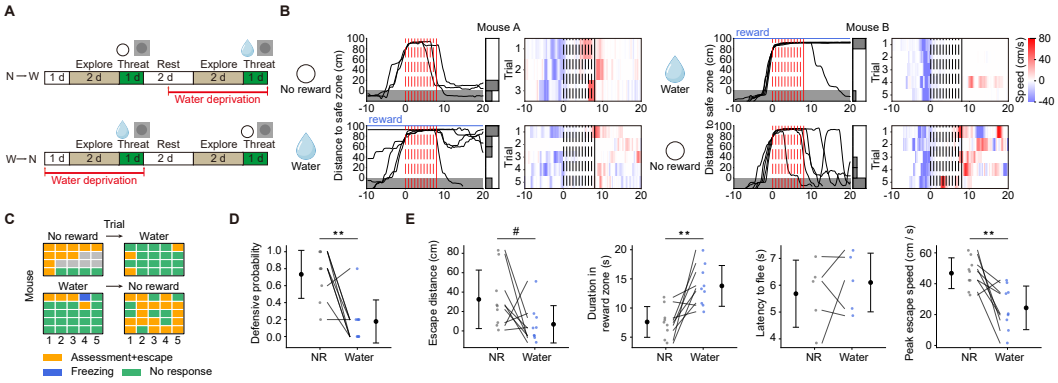

Figure S6: **Reward modulation of defensive behavior to looming stimuli in the same mouse.** (A) Experimental timeline illustrating how water reward influences innate decision-making within the same animal. (B) Distance to the safe zone and locomotion speed towards the safe zone across trials in response to low-contrast looming stimuli with and without water reward in two example mice. Left: no-reward condition followed by water-reward condition; Right: water-reward condition followed by no-reward condition. (C) Decision patterns of nine mice across two sessions with 5 trials for each. Gray squares indicate trials where the mouse did not enter the arena within 30 minutes. (D) Defensive probability in no-reward and water-reward conditions. N = 9 mice, paired *t*-test. (E) Escape distance under threat, duration in the reward zone, latency to flee, and peak escape speed in no-reward and water-reward conditions. N = 5 mice for latency to flee and 9 mice for other measures, paired *t*-test, two-sided. #$p < 0.1$, *$p < 0.05$, **$p < 0.01$.

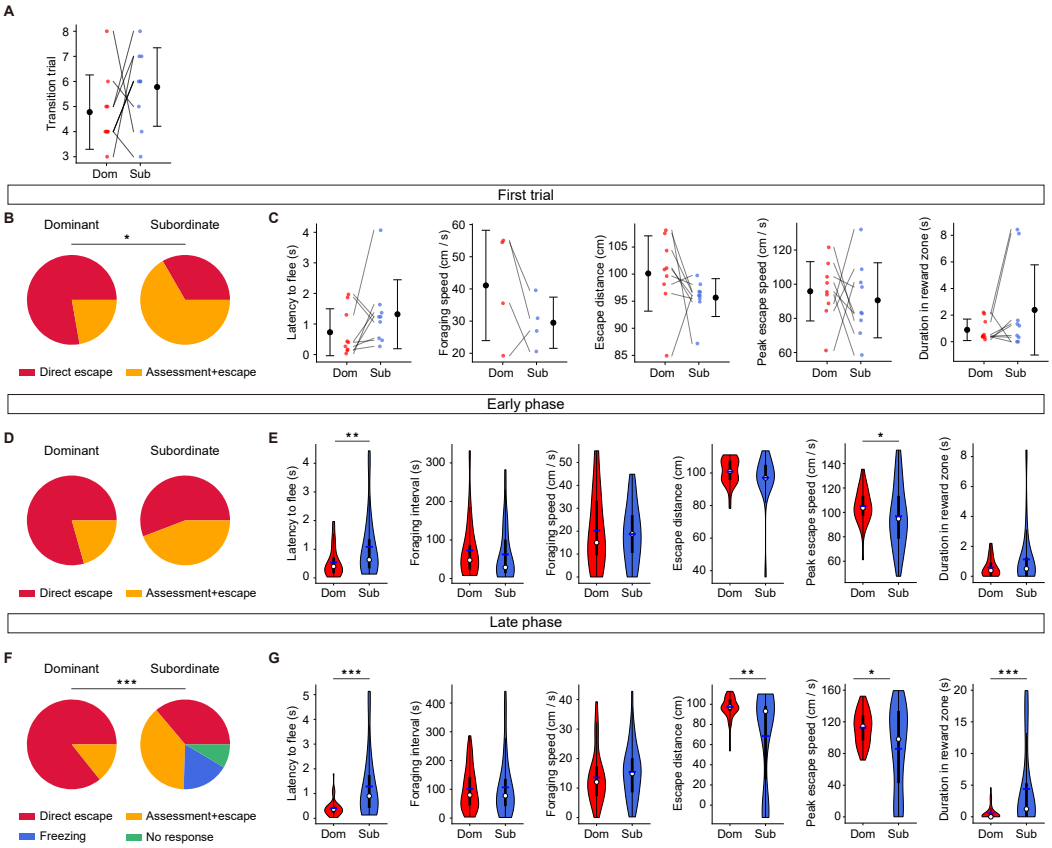

Figure S7: **Behavioral responses to looming stimuli for dominant and subordinate mice in different phases.** (A) Transition trial marking the start of the late phase for dominant and subordinate mice. N = 9 pairs. (B) Behavioral decisions for dominant and subordinate mice during their first exposure to threat. Stuart-Maxwell test. N = 9 pairs. (C) Latency to flee, foraging speed, escape distance under threat, peak escape speed, and duration in the reward zone during the first threat exposure. N = 4 pairs for foraging speed; N = 9 pairs for other features. Paired *t* test (D) Behavioral decisions for dominant and subordinate mice in the early phase. Chi-squared test. N = 34, 43 trials, respectively. (E) Violin plots showing latency to flee, average foraging interval, foraging speed, escape distance under threat, peak escape speed, and duration in the reward zone for dominant and subordinate mice in the early phase. N = 34, 43 trials, respectively. Mann-Whitney-Wilcoxon test. (F) Behavioral decisions for dominant and subordinate mice in the late phase. Chi-squared test. N = 56, 47 trials, respectively. (G) Violin plots showing latency to flee, average foraging interval, foraging speed, escape distance under threat, peak escape speed, and duration in the reward zone for dominant and subordinate mice in the late phase. N = 56, 35 trials for latency to flee; N = 56, 47 trials for other measures. Mann-Whitney-Wilcoxon test. $^{*}p < 0.05$, $^{**}p < 0.01$, $^{***}p < 0.001$.

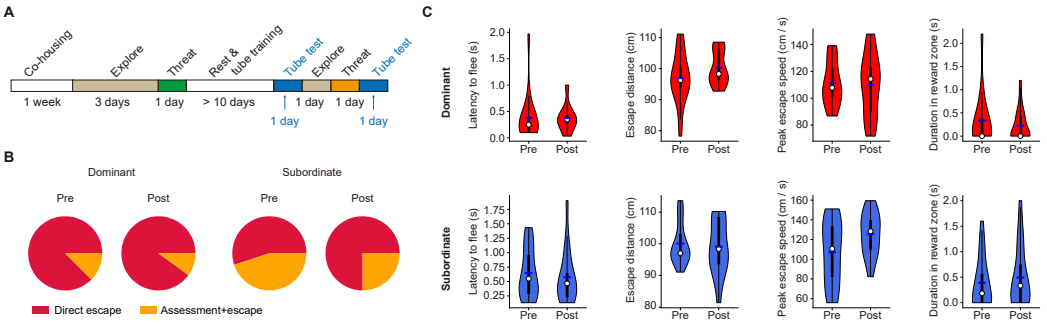

Figure S8: **Comparison of behavioral responses to looming stimuli before and after the tube test.** (A) Schematic timeline of the looming experiments before and after the tube test. (B) Behavioral decisions for dominant and subordinate mice before and after the tube test. Chi-squared test. Dominant: N = 16 (pre) and 20 (post) trials from 4 mice; Subordinate: N = 20 (pre) and 16 (post) trials from 4 mice. (C) Violin plots showing latency to flee, escape distance under threat, peak escape speed, and duration in the reward zone for dominant (top) and subordinate (bottom) mice before and after the tube test. Mann-Whitney-Wilcoxon test.

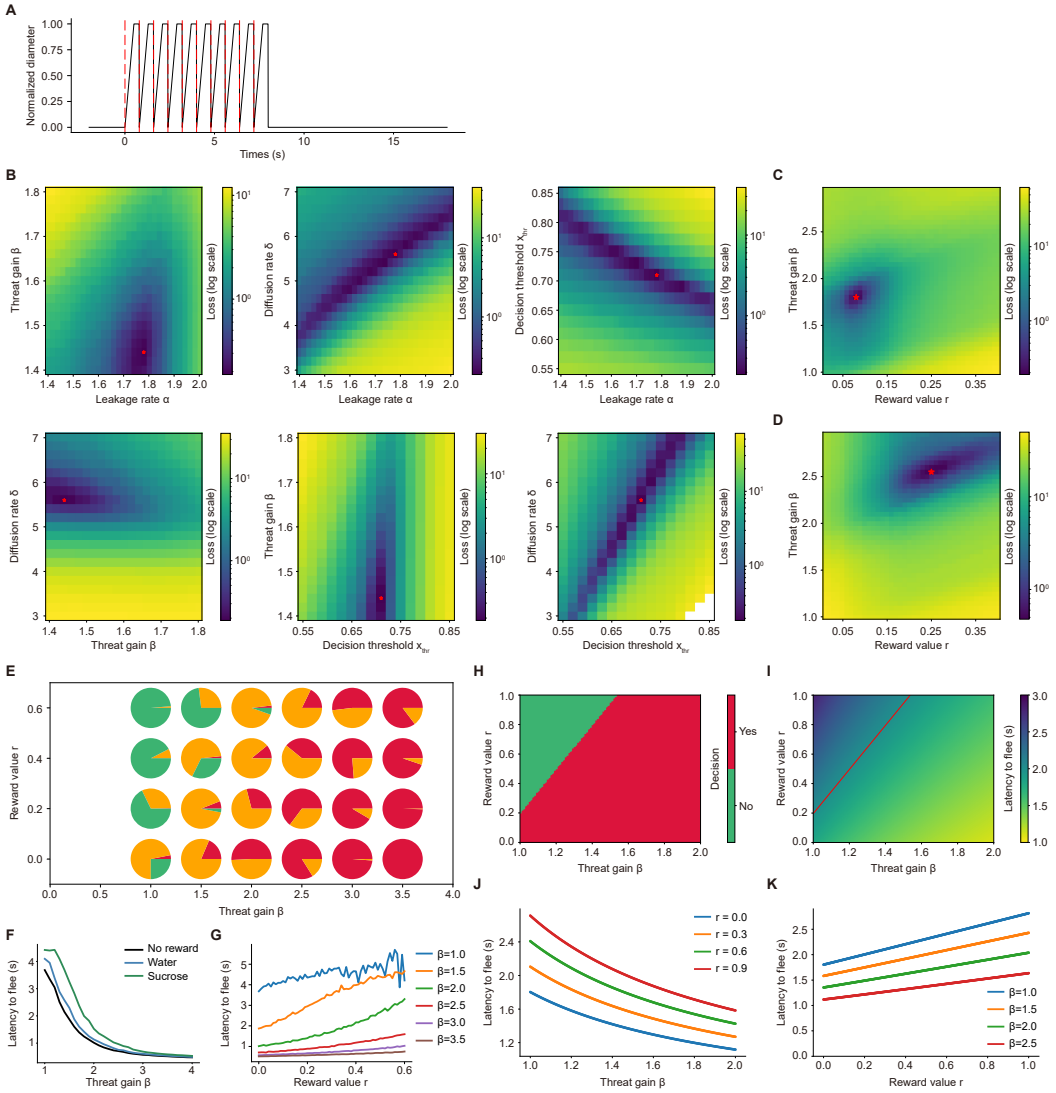

Figure S9: **Fitting loss in the drifting–diffusion leaky integrator model.** (A) Temporal profile of the normalized looming stimulus diameter. (B) Loss landscapes across the parameter space for estimating the leakage rate, high-contrast threat gain, diffusion rate, and decision threshold during the first-stage fitting. Red stars indicate the optimal parameter estimates based on experimental data in the late phase of the reward-related paradigm under the no-reward condition. (C) Loss landscapes across the parameter space for estimating the reward value and high-contrast threat gain under the water-reward condition. Red stars mark the optimal fits to experimental data in the late phase of the reward-related paradigm. (D) Same as (C), for the sucrose-reward condition. (E) Model-predicted distribution of decisions across threat gain and reward values. (F) Predicted latency to flee as a function of threat gain for varying reward values. (G) Predicted latency to flee as a function of reward value for varying threat gain. (H–I) Decisions and latency to flee across threat gain and reward values predicted by a simplified deterministic model. (J–K) Same as (F–G), but for the simplified deterministic model.

References

Amir, A., Lee, S.-C., Headley, D. B., Herzallah, M. M., and Pare, D. (2015). Amygdala signaling during foraging in a hazardous environment. *Journal of Neuroscience*, 35(38):12994–13005.

Andermann, M. L., Kerlin, A. M., and Reid, C. (2010). Chronic cellular imaging of mouse visual cortex during operant behavior and passive viewing. *Frontiers in Cellular Neuroscience*, 4.

Anderson, D. J. and Adolphs, R. (2014). A framework for studying emotions across species. *Cell*, 157(1):187–200.

Barnes, C. A. (1979). Memory deficits associated with senescence: a neurophysiological and behavioral study in the rat. *Journal of Comparative and Physiological Psychology*, 93(1):74–104.

Baruchin, L. J., Alleman, M., and Schröder, S. (2023). Reward modulates visual responses in the superficial superior colliculus of mice. *Journal of Neuroscience*, 43(50):8663–8680.

Benavidez, N. L., Bienkowski, M. S., Zhu, M., Garcia, L. H., Fayzullina, M., Gao, L., Bowman, I., Gou, L., Khanjani, N., Cotter, K. R., Korobkova, L., Becerra, M., Cao, C., Song, M. Y., Zhang, B., Yamashita, S., Tugangui, A. J., Zingg, B., Rose, K., Lo, D., Foster, N. N., Boesen, T., Mun, H.-S., Aquino, S., Wickersham, I. R., Ascoli, G. A., Hintiryan, H., and Dong, H.-W. (2021). Organization of the inputs and outputs of the mouse superior colliculus. *Nature Communications*, 12(1):4004.

Bravo-Rivera, C., Roman-Ortiz, C., Brignoni-Perez, E., Sotres-Bayon, F., and Quirk, G. J. (2014). Neural structures mediating expression and extinction of platform-mediated avoidance. *Journal of Neuroscience*, 34(29):9736–9742.

Buck, L. (1966). Reaction time as a measure of perceptual vigilance. *Psychological Bulletin*, 65(5):291–304.

Burgess, C. P., Lak, A., Steinmetz, N. A., Zatka-Haas, P., Reddy, C. B., Jacobs, E. A. K., Linden, J. F., Paton, J. J., Ranson, A., Schröder, S., Soares, S., Wells, M. J., Wool, L. E., Harris, K. D., and Carandini, M. (2017). High-yield methods for accurate two-alternative visual psychophysics in head-fixed mice. *Cell Reports*, 20(10):2513–2524.

Calvin, O. L., Erickson, M. T., Walters, C. J., and Redish, A. D. (2025). Dorsal hippocampus represents locations to avoid as well as locations to approach during approach-avoidance conflict. *PLOS Biology*, 23(1):e3002954.

Campagner, D., Vale, R., Tan, Y. L., Iordanidou, P., Pavón Arocas, O., Claudi, F., Stempel, A. V., Keshavarzi, S., Petersen, R. S., Margrie, T. W., and Branco, T. (2023). A cortico-collicular circuit for orienting to shelter during escape. *Nature*, 613(7942):111–119.

Caraco, T., Martindale, S., and Pulliam, H. R. (1980). Avian flocking in the presence of a predator. *Nature*, 285(5764):400–401.

Choi, J.-S. and Kim, J. J. (2010). Amygdala regulates risk of predation in rats foraging in a dynamic fear environment. *Proceedings of the National Academy of Sciences*, 107(50):21773–21777.

Cohen, J. Y., Haesler, S., Vong, L., Lowell, B. B., and Uchida, N. (2012). Neuron-type-specific signals for reward and punishment in the ventral tegmental area. *Nature*, 482(7383):85–88.

Comoli, E., Coizet, V., Boyes, J., Bolam, J. P., Canteras, N. S., Quirk, R. H., Overton, P. G., and Redgrave, P. (2003). A direct projection from superior colliculus to substantia nigra for detecting salient visual events. *Nature Neuroscience*, 6(9):974–980.

Comoli, E., Das Neves Favaro, P., Vautrelle, N., Leriche, M., Overton, P. G., and Redgrave, P. (2012). Segregated anatomical input to sub-regions of the rodent superior colliculus associated with approach and defense. *Frontiers in Neuroanatomy*, 6.

Constantinople, C. M., Piet, A. T., and Brody, C. D. (2019). An analysis of decision under risk in rats. *Current Biology*, 29(12):2066–2074.

De Franceschi, G., Vivattanasarn, T., Saleem, A., and Solomon, S. (2016). Vision guides selection of freeze or flight defense strategies in mice. *Current Biology*, 26(16):2150–2154.

Edwards, D. H. and Kravitz, E. A. (1997). Serotonin, social status and aggression. *Current Opinion in Neurobiology*, 7(6):812–819.

Evans, D. A., Stempel, A. V., Vale, R., and Branco, T. (2019). Cognitive control of escape behaviour. *Trends in Cognitive Sciences*, 23(4):334–348.

Evans, D. A., Stempel, A. V., Vale, R., Ruehle, S., Lefler, Y., and Branco, T. (2018). A synaptic threshold mechanism for computing escape decisions. *Nature*, 558(7711):590–594.

Fanselow, M. S. and Lester, L. S. (1988). A functional behavioristic approach to aversively motivated behavior: predatory imminence as a determinant of the topography of defensive behavior. In Bolles, R. C. and Beecher, M. D., editors, *Evolution and Learning*, pages 185–212. Lawrence Erlbaum Associates.

Gallistel, C. R., Fairhurst, S., and Balsam, P. (2004). The learning curve: Implications of a quantitative analysis. *Proceedings of the National Academy of Sciences*, 101(36):13124–13131.

Gibson, W. T., Gonzalez, C. R., Fernandez, C., Ramasamy, L., Tabachnik, T., Du, R. R., Felsen, P. D., Maire, M. R., Perona, P., and Anderson, D. J. (2015). Behavioral responses to a repetitive visual threat stimulus express a persistent state of defensive arousal in *drosophila*. *Current Biology*, 25(11):1401–1415.

Hayden, B. Y. (2018). Economic choice: the foraging perspective. *Current Opinion in Behavioral Sciences*, 24:1–6.

Hayden, B. Y., Pearson, J. M., and Platt, M. L. (2011). Neuronal basis of sequential foraging decisions in a patchy environment. *Nature Neuroscience*, 14(7):933–939.

Kahneman, D. and Tversky, A. (1979). Prospect theory: an analysis of decision under risk. *Econometrica*, 47(2):263–291.

Kingsbury, L., Huang, S., Wang, J., Gu, K., Golshani, P., Wu, Y. E., and Hong, W. (2019). Correlated neural activity and encoding of behavior across brains of socially interacting animals. *Cell*, 178(2):429–446.e16.

Kleiman, M., Bodek, S., and Eilam, D. (2014). Who are the bosses? Group influence on the behavior of voles following owl attack. *Behavioural Processes*, 108:183–190.

Krasne, F. B., Shamsian, A., and Kulkarni, R. (1997). Altered excitability of the crayfish lateral giant escape reflex during agonistic encounters. *Journal of Neuroscience*, 17(2):709–716.

Krauzlis, R. J., Lovejoy, L. P., and Zénon, A. (2013). Superior colliculus and visual spatial attention. *Annual Review of Neuroscience*, 36(1):165–182.

Lenzi, S. C., Cossell, L., Grainger, B., Olesen, S. F., Branco, T., and Margrie, T. W. (2022). Threat history controls flexible escape behavior in mice. *Current Biology*, 32(13):2972–2979.

Li, C., Kühn, N. K., Alkislar, I., Sans-Dublanc, A., Zemmouri, F., Paesmans, S., Calzoni, A., Ooms, F., Reinhard, K., and Farrow, K. (2023). Pathway-specific inputs to the superior colliculus support flexible responses to visual threat. *Science Advances*, 9(35):eade3874.

Li, Y.-t., Turan, Z., and Meister, M. (2020). Functional architecture of motion direction in the mouse superior colliculus. *Current Biology*, 30(17):3304–3315.e4.

Liden, W. H. and Herberholz, J. (2008). Behavioral and neural responses of juvenile crayfish to moving shadows. *The Journal of Experimental Biology*, 211(Pt 9):1355–1361.

Liu, Z., Zhou, J., Li, Y., Hu, F., Lu, Y., Ma, M., Feng, Q., Zhang, J.-E., Wang, D., Zeng, J., Bao, J., Kim, J.-Y., Chen, Z.-F., El Mestikawy, S., and Luo, M. (2014). Dorsal raphe neurons signal reward through 5-HT and glutamate. *Neuron*, 81(6):1360–1374.

Lorenz, K. Z. (1950). The comparative method in studying innate behavior patterns. *Symposia of the Society for Experimental Biology*, 4:221–268.

Mathis, A., Mamidanna, P., Cury, K. M., Abe, T., Murthy, V. N., Mathis, M. W., and Bethge, M. (2018). DeepLabCut: markerless pose estimation of user-defined body parts with deep learning. *Nature Neuroscience*, 21(9):1281–1289.

Meister, M. (2022). Learning, fast and slow. *Current Opinion in Neurobiology*, 75:102555.

Miyazaki, K., Miyazaki, K. W., and Doya, K. (2011). Activation of dorsal raphe serotonin neurons underlies waiting for delayed rewards. *Journal of Neuroscience*, 31(2):469–479.

Mooney, R. D., Huang, X., Shi, M. Y., Bennett-Clarke, C. A., and Rhoades, R. W. (1996). Serotonin modulates retinotectal and corticotectal convergence in the superior colliculus. *Progress in Brain Research*, 112:57–69.

Morris, R. (1984). Developments of a water-maze procedure for studying spatial learning in the rat. *Journal of Neuroscience Methods*, 11(1):47–60.

Moscarello, J. M. and LeDoux, J. E. (2013). Active avoidance learning requires prefrontal suppression of amygdala-mediated defensive reactions. *Journal of Neuroscience*, 33(9):3815–3823.

Mowrer, O. H. and Lamoreaux, R. R. (1946). Fear as an intervening variable in avoidance conditioning. *Journal of Comparative Psychology*, 39(1):29–50.

Raleigh, M. J., McGuire, M. T., Brammer, G. L., Pollack, D. B., and Yuwiler, A. (1991). Serotonergic mechanisms promote dominance acquisition in adult male vervet monkeys. *Brain Research*, 559(2):181–190.

Rangel, A., Camerer, C., and Montague, P. R. (2008). A framework for studying the neurobiology of value-based decision making. *Nature Reviews Neuroscience*, 9(7):545–556.

Ratcliff, R. (1978). A theory of memory retrieval. *Psychological Review*, 85(2):59–108.

Rosenberg, M., Zhang, T., Perona, P., and Meister, M. (2021). Mice in a labyrinth show rapid learning, sudden insight, and efficient exploration. *eLife*, 10:e66175.

Schultz, W. (1998). Predictive reward signal of dopamine neurons. *Journal of Neurophysiology*, 80(1):1–27.

Schultz, W., Apicella, P., Scarnati, E., and Ljungberg, T. (1992). Neuronal activity in monkey ventral striatum related to the expectation of reward. *Journal of Neuroscience*, 12(12):4595–4610.

Shang, C., Chen, Z., Liu, A., Li, Y., Zhang, J., Qu, B., Yan, F., Zhang, Y., Liu, W., Liu, Z., Guo, X., Li, D., Wang, Y., and Cao, P. (2018). Divergent midbrain circuits orchestrate escape and freezing responses to looming stimuli in mice. *Nature Communications*, 9(1):1232.

Shang, C., Liu, Z., Chen, Z., Shi, Y., Wang, Q., Liu, S., Li, D., and Cao, P. (2015). A parvalbumin-positive excitatory visual pathway to trigger fear responses in mice. *Science*, 348(6242):1472–1477.

Small, W. S. (1901). Experimental Study of the Mental Processes of the Rat. II. *The American Journal of Psychology*, 12(2):206–239.

Steiner, A. P. and Redish, A. D. (2014). Behavioral and neurophysiological correlates of regret in rat decision-making on a neuroeconomic task. *Nature Neuroscience*, 17(7):995–1002.

Steinmetz, N. A., Zatka-Haas, P., Carandini, M., and Harris, K. D. (2019). Distributed coding of choice, action and engagement across the mouse brain. *Nature*, 576(7786):266–273.

Tammero, L. F. and Dickinson, M. H. (2002). Collision-avoidance and landing responses are mediated by separate pathways in the fruit fly, Drosophila melanogaster. *The Journal of Experimental Biology*, 205(Pt 18):2785–2798.

Tremblay, L. and Schultz, W. (2000). Reward-related neuronal activity during go-nogo task performance in primate orbitofrontal cortex. *Journal of Neurophysiology*, 83(4):1864–1876.

Truong, C., Oudre, L., and Vayatis, N. (2020). Selective review of offline change point detection methods. *Signal Processing*, 167:107299.

Vale, R., Evans, D. A., and Branco, T. (2017). Rapid spatial learning controls instinctive defensive behavior in mice. *Current Biology*, 27(9):1342–1349.

Wagner, M. J., Kim, T. H., Savall, J., Schnitzer, M. J., and Luo, L. (2017). Cerebellar granule cells encode the expectation of reward. *Nature*, 544(7648):96–100.

Wallace, D. J., Greenberg, D. S., Sawinski, J., Rulla, S., Notaro, G., and Kerr, J. N. D. (2013). Rats maintain an overhead binocular field at the expense of constant fusion. *Nature*, 498(7452):65–69.

Wang, F., Zhu, J., Zhu, H., Zhang, Q., Lin, Z., and Hu, H. (2011). Bidirectional control of social hierarchy by synaptic efficacy in medial prefrontal cortex. *Science*, 334(6056):693–697.

Wei, P., Liu, N., Zhang, Z., Liu, X., Tang, Y., He, X., Wu, B., Zhou, Z., Liu, Y., Li, J., Zhang, Y., Zhou, X., Xu, L., Chen, L., Bi, G., Hu, X., Xu, F., and Wang, L. (2015). Processing of visually evoked innate fear by a non-canonical thalamic pathway. *Nature Communications*, 6:6756.

Woolrych, A., Vautrelle, N., Reynolds, J. N. J., and Parr-Brownlie, L. C. (2021). Throwing open the doors of perception: The role of dopamine in visual processing. *European Journal of Neuroscience*, 54(6):6135–6146.

Yang, X., Liu, Q., Zhong, J., Song, R., Zhang, L., and Wang, L. (2020). A simple threat-detection strategy in mice. *BMC Biology*, 18(1):93.

Ydenberg, R. C. and Dill, L. M. (1986). The economics of fleeing from predators. *Advances in the Study of Behavior*, 16:229–249.

Yeh, S.-R., Musolf, B. E., and Edwards, D. H. (1997). Neuronal adaptations to changes in the social dominance status of crayfish. *Journal of Neuroscience*, 17(2):697–708.

Yilmaz, M. and Meister, M. (2013). Rapid innate defensive responses of mice to looming visual stimuli. *Current Biology*, 23(20):2011–2015.

Zhong, J., Liu, Q., Yang, X., Su, J., Li, X., Luo, M., and Wang, L. (2023). Mice learn from the predator-attack experience to accelerate flight behavior via optimizing the strategy of environment exploration. *Biochemical and Biophysical Research Communications*, 665:26–34.

Zhou, Z., Liu, X., Chen, S., Zhang, Z., Liu, Y., Montardy, Q., Tang, Y., Wei, P., Liu, N., Li, L., Song, R., Lai, J., He, X., Chen, C., Bi, G., Feng, G., Xu, F., and Wang, L. (2019). A VTA GABAergic neural circuit mediates visually evoked innate defensive responses. *Neuron*, 103(3):473–488.e6.